NUMERICAL INVESTIGATION OF THERMAL MANAGEMENT IN PHOTOVOLTAIC CELLS WITH PHASE CHANGING MATERIALS (PCM) AND HIGH CONDUCTIVITY INSERTS

A Thesis Submitted to

the Graduate School of Engineering and Science of

İzmir Institute of Technology

in Partial Fulfilment of the Requirement of the Degree of

MASTERS OF SCIENCE

in Mechanical Engineering

by

Sylevaster KYALIGONZA

June 2021

İZMİR

ACKNOWLEDGMENT

First and foremost, I thank almighty God, the omnipotent, the Most Gracious, the Most Merciful, God of heavens and earth, the King of all Kings, God the Father, the Son, the Holy Spirit, God of Abraham, and his descendants for empowering us with the most precious gift of life. Through him, in him, and with him we live. All glory and honour upon him forever and ever.

My heartfelt appreciation goes to my academic parent and at the same time my thesis advisor Assoc. Prof. Erdal ÇETKİN of the Department of Mechanical Engineering at the İzmir Institute of Technology. He always opened doors for me whenever I reached on him for any academic assistance and guidance. He made the progressive journey in this research appear easy and simple. He owned the research and always encouraged by his verbal communication of “let us” instead of “you should”. May God continue using him in his academic career. My special appreciation goes to Assoc. Prof. Ünver Özkol, the Head of the Department of Mechanical Engineering of the İzmir Institute of Technology. Additionally, I would like to thank the entire teaching and non-teaching of the Department of Mechanical Engineering of the İzmir Institute of Technology especially my course instructors: Assoc. Prof. H. Seçil Artem, Assoc. Prof. Murat Barışık, and Assoc. Prof. Kasım Toprak. It is because of their efforts and passionate encouragement that I emerged through this research. I am gratefully indebted to some of my fellow students in various departments of İzmir Institute of Technology for their valuable inputs on this thesis and research.

With special thanks, I would also like to thank Turkey's Presidency for Turks Abroad and Related Communities (YTB), for fully sponsoring my education and memorable stay at the İzmir Institute of Technology.

I express my heartfelt gratitude to the family of Mr. & Mrs. Kyaligonza Sylevaster, the family where I belong, for their unending love and support in my education career. Thank you.

ABSTRACT

NUMERICAL INVESTIGATION OF THERMAL MANAGEMENT IN PHOTOVOLTAIC CELLS WITH PHASE CHANGING MATERIALS (PCM) AND HIGH CONDUCTIVITY INSERTS

Photovoltaic cells' electrical conversion efficiency from incident solar radiation heavily depends on the cell temperature. A novel thermal management strategy aimed at keeping the cell temperature in the same order to maximize PV cell electrical conversion efficiency is proposed in this study. The study compares four solar module configurations: a conventional photovoltaic module (PVT module), a hybrid of conventional with PCM (PVT/PCM-I), an internally finned configuration with PCM (PVT/PCM-II), and a configuration where the bottom surface of PVT/PCM-II was cooled via convection (PVT/PCM-III). The developed 3D numerical model was solved via ANSYS software involving the solar ray tracing radiation model for incident solar radiations and a transient melting-solidification thermo-fluid model for modelling of the PCM. Numerical results were validated by comparing them against experimental results published in the literature. Results show that the conversion efficiency of PV cells reaches 16.84%, 18.65%, 18.83%, and 18.98% after 120 minutes for PVT module, PVT/PCM-I, PVT/PCM-II, and PVT/PCM-III, respectively while the specific electrical power produced reaches 75.30W/m^2, 83.39W/m^2, 84.19W/m^2, and 89.42W/m^2 for solar radiation of 540W/m^2 and 26°C ambient temperature. A 5 mm increase in the fin height for PVT/PCM-II results in a 0.22% increase in efficiency while a 0.5m/s increase in the inlet velocity of the cooling air for PVT/PCM-III results in about 0.06% efficiency increase. Furthermore, performance evaluation of PVT/PCM-III was carried out with sample weather data of the Indian Institute of Technology-Delhi and the Algiers site. The hourly average of overall conversion efficiency for the respective sites reaches 16.70% and 16.84% for a conventional PV module and 19.04% and 19.19% for PVT/PCM-III where the conversion efficiency increases by 14% and 13.7% respectively.

ÖZET

FAZ DEĞİŞTİREN MALZEMELER (FDM) VE YÜKSEK İLETİMLİ EKLENTİLER İLE FOTOVOLTAİK HÜCRELERİN ISIL YÖNETİMİNİN SAYISAL OLARAK ARAŞTIRILMASI

Fotovoltaik hücrelerin elektriği güneş radyasyonundan üretmesindeki dönüşüm verimliliği büyük ölçüde hücre sıcaklığına bağlıdır. Bu çalışmada fotovoltaik (PV) hücre elektrik dönüşüm verimliliğini en üst düzeye çıkarmak için hücre sıcaklığını aynı seviyede tutmayı amaçlayan yeni bir ısıl yönetim stratejisi önerildi. Çalışma dört güneş modülü konfigürasyonunu karşılaştırmaktadır: geleneksel fotovoltaik modülü (PVT modülü), faz değiştiren malzeme (PCM) ile geleneksel sistemin hibridi (PVT / PCM-I), PCM içerisinde kanatçıklar (PVT / PCM-II) ve PVT / PCM-II'nin alt yüzeyinin taşınım (PVT / PCM-III) ile soğutulduğu yapılar. Geliştirilen 3B sayısal model, güneş radyasyonlarının izlenmesini içeren radyasyon modelini ve PCM'nin modellenmesi için erime-katılaşma termo-akışkan modellerini içermektedir ve ANSYS yazılımı aracılığıyla çözülmüştür. Sayısal sonuçlar literatürde yayınlanan deneysel sonuçlarla karşılaştırılarak doğrulanmıştır.

Sonuçlar, PVT, PVT/PCM-I, PVT/PCM-II, ve PVT/PCM-III için 120 dakika sonra dönüşüm verimliliğinin sırasıyla %16.84, %18.65, %18.83 ve %18.98'e ulaştığını göstermektedir. Üretilen elektrik gücü yine sırasıyla 75.30W/m^2, 83.39W/m^2, 84.19W/m^2 ve 89,42W/m2'ye, 540W/m^2 ışınım akısı ve 26°C ortam sıcaklığındaki durum için ulaşır. PVT/PCM-II için kanatçık yüksekliğindeki 5 mm'lik artış verimlilikte %0.22'lik bir artışa neden olurken, PVT/PCM-III için soğutma havasının giriş hızında 0.5 m/s'lik bir artış yaklaşık %0.06 verimlilik artışına neden olur. Ayrıca, PVT / PCM-III'ün performans değerlendirmesi, Hindistan Teknoloji Enstitüsü-Delhi ve Cezayir sitelerinin örnek hava durumu verileri ile doğrulanmıştır. İlgili siteler için genel dönüşüm verimliliğinin saatlik ortalaması, geleneksel bir PV modülü için dönüşüm verimliliği %16.70 ve %16.84'e ve PVT / PCM-III için %19.04 ve %19.19'a ulaşır, bu ise dönüşüm verimliliğinin sırasıyla %14 ve %13.7 arttığını gösterir.

TABLE OF CONTENT

LIST OF FIGURES

Figure **Page**

Figure **Page**

LIST OF TABLES

Table **Page**

NOMENCLATURE

Abbreviations

AM	Air mass
BIPV	Building Integrated photovoltaic
CFD	Computational fluid mechanics
CPV	Concentrated photovoltaic
CSP	Concentrated solar power
EAHE	Earth-to-air heat exchanger
EGS	Engineered geothermal systems
EUT	Earth's undisturbed temperature
EVA	Ethylene-Vinyl acetate
GDP	Growth domestic product
GW	Giga watt
HC	Higher capacity
HOMO	Highest occupied molecular orbital
IEA	International energy Agency
LHS	Latent heat storage
LUMO	Lowest Unoccupied molecular orbital
MJ	Multi-junction
Np	Number of parallel pipes.
NTU	Number of transfer units
OECD	Organization for Economic cooperation and development.
PAR	Photosynthetically active radiation.
PCM	Phase change materials
PRESTO	PREssure Staggering Option
PV	Photovoltaic
PVC	Polyvinyl chloride
PVF	Polyvinyl fluoride
PVT	Photovoltaic thermal
RT	Rubitherm
SE4ALL	Sustainable energy for all
SHS	Sensible heat storage

SIMPLE	Semi implicit pressure linked equation
SSA	Sub-Sahara Africa
STC	Standard test conditions
TFEC	Total Final energy consumption
TIM	Thermal interface material
WWEA	World wind energy association.

Subscripts

a	air
amb	ambient
avg	average
e	EVA
F	Final
f	Fluid
g	glass
i	initial
in	inlet
l	Liquid state
lm	logarithmic mean
m	molten state
n	normal coordinate at interface
out	outlet
ref	reference
sc	solar cell
s	solid state
th	thermal
t	turbulent
w	wind

Greek letters

α	Absorptivity
β	Thermal expansion coefficient [K^{-1}]
δ	Thickness [mm]
η	Efficiency

μ	Dynamic viscosity [kg m^{-1} s^{-1}]
ρ	Density [kg m^{-3}]
τ	Transmissivity
λ	Liquid fraction

Symbols

C_p	Specific heat capacity [kJkg^{-1} K^{-1}]
D	Diameter [m]
∇	Del operator
g	Acceleration due to gravity[ms^{-2}]
H	Enthalpy [J]
k	Thermal conductivity [$Wm^{-1}K^{-1}$]
L	Latent heat of fusion of phase change material [kJkg^{-1}]
m	Phase change material mass [kg]
Q	Heat absorbed by phase change material [kJ]
T	Temperature [°C]
T_m	Melting point of phase change material[°C]
t_{sc}	Average PV cells' temperature [K]
v	Velocity [ms^{-1}]
Γ́	Interface between the solid and fluid.

CHAPTER 1

INTRODUCTION

Energy usage is an essential part of the modern lifestyle due to its requirement for production, transportation, entertainment, and actually for all the activities. All the moving animals and even non-moving plants rely on converting energy from one form to another to live. Therefore, life is associated with energy conversion from one form to another such as chemical energy stored in food to mechanical energy to enable us to move on the landscape or replenish the cells in our bodies. However, the conversion of energy from one form to another comes with the cost of entropy generation and its effects on the environment. Even though each conversion method is generating entropy, some are affecting the environment more than others such as electricity generation from non-renewable sources (fossil fuels) [1].

1.1 Background

Economies entirely rely on energy from production to any kind of services, so adequate energy availability in a given country or entity plays the utmost importance to its growth, productivity, and development[2]. This energy is exploited from either renewable or non-renewable sources. The latter suffers from depletion despite their high energy densities and include petroleum and its by-products. fossil fuels (natural gas and coal), and radioactive elements. The renewables include resources with an instantaneous regeneration and cannot be depleted to a finite quantity. They are inexhaustible such as geothermal, tidal, wind, hydroelectricity, and solar. These sources have a relatively low energy potential compared to non-renewable sources. They attract attention because they are inexhaustible [3].

The energy demand increased by an estimate of 2.3% in 2018. The increase was a result of global economic growth of about 3.7%, and in some regions, it was due to environmental temperature characterized by increased heating and cooling demand. Developed countries of China, India, and the United States accounted for nearly 70% of this increased demand. The

growth in energy demand has raised fossil fuel consumption and an estimated 1.7% carbon dioxide (CO2) emissions increase was recorded. In the previous year, it was estimated that 18.1% of the total energy consumed by end-users globally (total final energy consumption (TFEC)) was attributed to renewable energy with modern renewable technologies supplying 10.6%, corresponding to a 4.4% growth increment compared to 2016 [4].

The question of global energy deficiencies has taken the attention of most researchers, scientists, and industries working in energy-related disciplines. Amongst all the energy sources, whether renewable or not, solar energy has always been at the peak of researchers' interests [3]. The solar energy provided by the sun is seen and manifested in plants in a process called photosynthesis which is primarily affecting the food sources. With a need to curb the ever-raising rates of global warming in the world, solar energy became an attractive venture because of its low adverse effects on nature amongst all other sources [4].

By the year 2008, the production of photovoltaic cells annually under standard test conditions nearly exceeded 7.9 GW, resulting in over 40% production growth throughout 10 years despite their low percentage contribution of 0.1% to the annual global electricity production [5]. By 2020, the annual production of PV cells was expected to be 100GWp with silicon-based solar cells as the highest contributor to the market. Silicon, unlike other materials, has no negative effects on the environment and its abundance on earth of 26% of crustal material gives it a comparative advantage over other materials in the PV industry[6].

In recent years, commercial and domestic solar energy usage has risen and continues to raise [1], [4], [7]. In less developed countries, however, there is high domestic use of solar energy than commercial use. This continuous growth in global energy demand requires new and advanced technologies to be implemented for harvesting solar energy. Solar energy can be harvested in two distinct ways: solar photovoltaic (PV) systems that involve the direct conversion of electricity from incident solar radiation and solar thermal systems in which extracted energy from incident solar radiation is converted into heat for heating applications [2]. In most thermal systems, power cycles are employed to convert thermal energy into mechanical work. Solar panels enable the heat to be used directly as process heat or supply to a Rankine cycle for electricity generation. Even though the conversion efficiency of solar

radiation to heat is comparatively high, if it is coupled with the Rankine cycle, system efficiency becomes the multiplication of Rankine cycle efficiency and heat conversion efficiency. For direct heating applications, the efficiency of solar thermal systems reaches up to 60%, requiring high temperature applications and lower efficiency values between 12% and 20% are registered in direct power generation applications unless concentration technologies are adopted [2], [8].

To convert sunlight into energy, a small, highly efficient optoelectronic device is used. This device is the solar cell, assumed as a “black box”, receiving sunlight, and emitting electrons. All solar cells must obey the following principles in their operation [3], [9], [10].

Ability to absorb incident radiation. Light absorption is a characteristic of the solar cell material and directly relates to the absorption spectrum of that material. The absorption spectrum is a function of the atomic and molecular structure of the material and is defined as a portion of the radiation absorbed by a particular material on which it is incident for a given range of frequencies. Ideally, the material for electricity generation in a solar cell corresponds to an absorption spectrum with an AM1.5 [9].

Ability to generate charge. When incident radiation falls on the solar cell surface, photocarriers (electrons and holes) are generated aided by energy provided by the sun. Such a process is possible in semiconductors basing on their electronic band structure [3].

Ability to transport the generated charge. As radiation strikes the generated electrons, they gain photon energy, allowing them to travel freely. However, because this movement is random, no current passes through the load. A driving force is required to make electrons flow unidirectionally[11][12]. In practice, a PN junction is a simple way to generate this driving force. When incident radiation reaches the N region of a PV cell's PN Junction, it penetrates and reaches the depletion zone, which is devoid of free electrons and holes. In the depletion area, this photon energy is sufficient to form electron-hole pairs. Electrons and holes are driven out of the depletion area by an electric field. The concentration of electrons in the N region and that of holes in the P region reaches such a high level that a potential difference develops between them. When a load is connected across them, electrons flow as photocurrent through the load.

For solar energy to be a better option to supporting off and on-grid power demands, a solar cell with very high conversion efficiency is fabricated without or with minimum material degradation. Over the past years, silicon-based especially thin-film cells have gained application due to escalation in manufacturing proficiency. Silicon-based solar cells are manufactured using the following decomposition techniques; Sputtering, thermal and e-beam evaporation, molecular beam epitaxy, close space sublimation, and metal-organic chemical vapor deposition. These techniques are costly and sophisticated thus resulting in an expensive production process and product costs too, become expensive[13]–[15].

Literature documents that only 5% to 40% of the incident solar radiation is converted into electricity while a portion of the remaining radiation is reflected and the other dissipated as thermal energy in a typical PV panel[16]. This heat generated raises the cell's temperature and in turn, reduces electrical conversion efficiency. On average, the efficiency of the PV cells takes orders of 26% for monocrystalline (Mono c-Si), 21% for polycrystalline silicon cells, 21.6% for thin-film cells, 21.4%, for Cadmium Telluride (Cd-Te) cells have and 11.8% for amorphous silicon cells[13]. Electricity generation from solar radiation is appealing because of no harmful emissions and the capability to be implemented as an off or on-grid power source. Generating electricity from the roof of houses during the day and then using electricity from the grid during the night minimize the electricity generation from other sources [17], [18]. In addition, in remote locations (without a grid) PV cells become a low-cost and reliable source if they are coupled with an energy storage unit such as a battery[18]. The conversion efficiency of the PV cells increased in recent years as their production cost decreased. For instance, the average efficiency of monocrystalline silicon PV cells increased from 4.5% in 1953 to the present 26% efficiency while the cost has reduced by approximately 87% in the last 25 years[5]. Even though the production costs have been decreasing over the years, they are not in the desired order as the manufacturing process requires advanced techniques[13], [14].

In this work, therefore, the focus is directed towards improving the electricity conversion efficiency of the polycrystalline solar cell by reducing its surface temperature while exposed to sunlight. Attention is placed on the use of phase-changing material for heat absorption. When the temperature of the PCM raises above its melting point, it melts while

absorbing sensible heat. Therefore, energy storage and release occur when PCM's temperature increases or decreases, respectively due to enthalpy change as the material changes phase. The latent heat energy storage is an isothermal process[19]. The performance of a PCM is enhanced by adding high conductive copper fins. The copper fins embedded in the PCM domain play two main advantages: improving the thermal conductivity of PCM by providing an extra surface area for heat transfer. This increases heat transfer inside the PCM. Fins too act as pressure relief passageways for molten PCM upon solidification.

1.2 Research objectives

The main objective for this study was to develop a numerical model investigating thermal management in photovoltaic cells with phase-changing materials (PCM) and high conductivity inserts.

The specific objectives include the following.

i. To systematically study the solar radiation modelling approach and software aided methods that predict the surface temperature of photovoltaic modules.
ii. To propose highly efficient materials and methods used in solar cell cooling to improve efficiency.
iii. To carry out performance analysis on the cell based on the numerical results, analysis parameters, and expressions.
iv. To ascertain the best environmental conditions under which the proposed cooling methods are efficient.

To achieve the above objectives, the developed computational models were subjected to the set boundary conditions and solved using a CFD software ANSYS 2020 R1 based on finite element techniques. The drawn computation domains were discretized in the 3D coordinate using ANSYS geometry design modeler and mesh generation software workbench. After defining the boundary surfaces, the generated mesh was exported to the fluent software. Irradiation analysis is based on solar ray tracing with the sun normal to the surface of the module (smart system) and assuming that the radiation incident on the panel is

uniformly distributed[20][21]. The study was conducted considering 4 PV module configurations namely PVT module, PVT/PCM-I, PVT/PCM-II, and PVT/PCM-III. PVT module was executed in fluent by adding an air duct underneath and using a very small inlet velocity representing a low convection heat transfer coefficient thus approximating the flow to be stagnant. PVT/PCM-I and PVT/PCM-II were executed by activating the melting and solidification model to enable the melting of RT35 phase-changing material. In addition to the melting and solidification model, PVT/PCM-III was executed by a turbulent Realizable K-epsilon model with standard wall functions. The mass, velocity, and energy equations were solved using the finite volume approach together with the enthalpy–porosity formulation. The pressure correction equation was solved using the PREssure STaggering Option (PRESTO) scheme, and the semi-implicit pressure-linked equation (SIMPLE) algorithm was employed for pressure-velocity coupling. The momentum and energy equations were solved using the quadratic upwind differencing (QUICK) scheme. All transient simulations were executed with the first-order implicit transient formulation. The above methods were suggested by M.Emam et al[20] for a better correlation between numerical and experimental data.

1.3 Structure of the thesis.

The presented thesis is arranged into six (6) chapters, as explained below:

Chapter 1: A brief background on solar energy and its adverse advantages over other renewable energy sources is presented. The chapter also briefly explains the key principles on which photovoltaic solar cells operate. Furthermore, the objectives together with the achieved milestone of the study are discussed.

Chapter 2: A Survey on the literature in energy fields is presented. An exploration of the energy demand, siting different energy sources is presented.

Chapter 3: The chapter includes an extended review of solar cell generations and ultimate efficiencies. An extended study on the use of phase change materials for thermal regulation in photovoltaic cells is presented.

Chapter 4: An extended description of the numerical model, modelling assumptions, and simulation procedures are discussed in this chapter. The selection of materials favourable to the intended system's output is presented here. The use of a CFD Ansys software with a solar ray tracing radiation model for modelling solar cells is presented along with validation of the numerical results.

Chapter 5: An extended discussion of the results of the simulation model is presented in this chapter. Furthermore, a verification of the PVT/PCM-III system's thermal performance is evaluated in this chapter.

Chapter 6: A summary of the concluding remarks and recommendations for the system's modifications for future studies is presented.

CHAPTER 2

ENERGY DEMAND, SUPPLY, AND UTILIZATION

As countries all around the world have painfully discovered, energy discovery and production are no longer as cheap as it once was. Whatever sort of energy used, it is well understood that obtaining new supplies is challenging and requires more people and material resources. It is, therefore, a human responsibility to plan for tomorrow's energy supply needs and appropriately manage them. Inadequate energy hinders economic growth and development and jeopardizes human subsistence while abundant energy supplies mean that there is an unnecessary expenditure of scarce resources.

2.1 Energy demand

In almost all developed and developing countries, human activities in their economies have absorbed whatever quantities of energy that producing firms have been able to supply. In some energy sources, however, provision of adequate energy may be hindered by resource limits as with fossil fuels, natural gas, and others, or financial constraints as with imported energy sources. It then becomes compulsory to understand the trends in energy demands as it makes planning for economic growth and development a realizable goal[22]. In a need to ascertain the supply of energy sources, several features of energy demand are crucial. First, one should look at the type of energy. As some countries develop towards a heavy industrial mix that relies on heavy oils/coal and base-load electric power (e.g., Korea), other countries, especially less developed ones focus on lighter energy sources since energy demands are directed to lighter industries, agriculture, and domestic use. Countries with large tourism industries employ solar in thermal management of buildings, lighting, and water heating while those countries that largely depend on food processing and textile may make use of large-scale biomass plants since food and textile industries require low-temperature heating[23][4].

Globally, the energy demand grows exponentially due to industrialization. This led to the discovery of alternative and traditional energy sources such as coal, natural gas, oil, and its by-products. Despite their adverse contribution to increased pollution and deterioration of human health, they have also extensively contributed to closing the gap between energy demand and energy supply[23][4] [24]. To curb the effect of pollution, renewable energy sources (RES) have been employed in recent years. In 2017, the maximum global renewable power capacity was estimated as 2195 GW, of which 53% was hydropower, 23% was wind energy, 18% was solar power, and 6% of other renewable sources, while by 2020, the deployment in solar exponentially increased (Fig.2.1)[24]. The expected installation of renewable energy by countries between the period of 2020-2030 is presented in Fig.2.2.

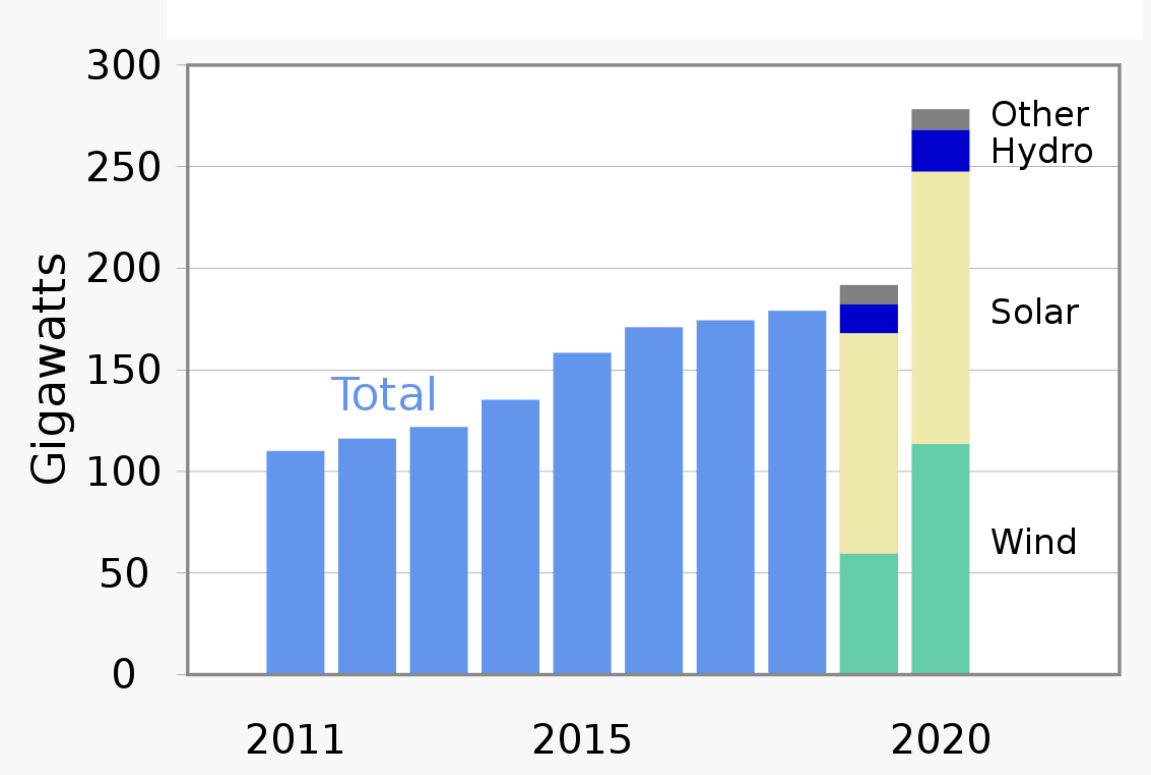

Figure 2.1:Global renewable energy capacity by 2020[24].

The rate of growth of global primary energy consumption has remained constant at 2.45 per year since 1850 and shows no signs of slowing[25]. Reduced energy demand, combined with increased efficiency, is often recognized as the most promising, quickest, cheapest, and safest method of reducing climate change and pollution. Attempts to curb

increased energy demand in the past have not been a success. The International Energy Agency (IEA), in collaboration with other organizations, has set and continues to set goals for lowering energy demand[23].

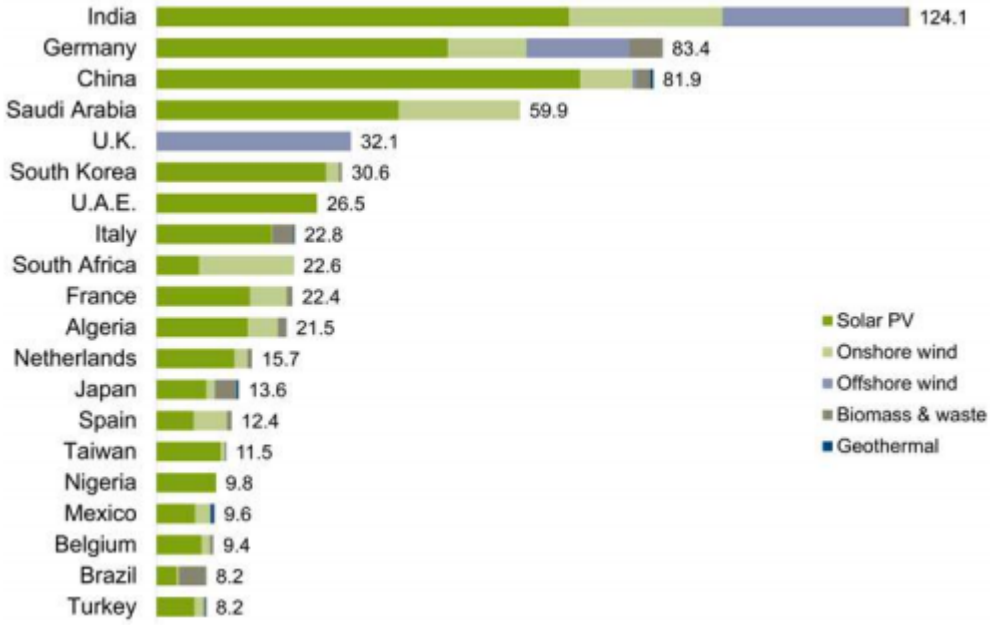

Figure 2.2:Renewable energy deployment expectations between 2020-2030[26].

Countries all over the world are imposing numerous ranges of policies to put in practice the long-term targets set by the European Commission for Energy demand reduction[23]. Approximately 3 billion people rely on traditional biomass for cooking and heating, according to 2010 estimates from the Organization for Economic Co-operation and Development (OECD) and the International Energy Agency (IEA). Around 20% of the world's population (1.4 billion people) does not have access to electricity, with 85 percent of those living in rural regions. It is also believed that more than a billion people can only access unreliable electricity networks [27].

Despite being gifted with the widest range of energy resources past its energy needs, Africa’s energy sector remains underdeveloped. It is believed that over 500 million Africans have no access to electricity with an additional 9 million of the population with no electricity access for almost 20 years[28]. According to the International Energy Agency (IEA), by 2002 only 13% of Africa’s population was electrified compared to the world average of 73%. This

makes Africa the least electrified of any other major region in the world. In almost all countries, energy consumption and electric usage remain low. It is cited that for more than a century ago an African uses less energy than a person from England would use. In 2000, commercial and non-commercial energy usage in North America was 280GJ, a value that is 11 times as much as the energy used in sub-Saharan Africa (25GJ)[28]. According to the International Energy Agency (IEA), Sub-Saharan Africa (SSA) alone has 99.6% of the African population without access to electricity. This reflects the significant discrepancies between African regions, which are mostly due to the continent's continuing imbalanced development of energy production and transportation infrastructures[27], as seen in Fig.2.3. Even though just 15% of South Africa's population does not have access to electricity, three-quarters of East Africans, half of West Africans, and the majority of Southern Africans do. The northern part of Africa's Gross Domestic Product (GDP) per capita is three to five times larger than any other region, and just about 2% of the residents lack access to electricity[1].To fill the energy gap in Africa, there is a need to address its energy sector with an utmost sense of urgency[7]. The only alternative energy resources abundantly available throughout the African continent include solar energy, wood and biomass, biogas, and wind energy.

The first step of understanding the exploitability of renewable energy sources is mapping their physical availability. In analysing the economically utilizable renewable energy resources, a thorough study of the current and possible energy infrastructure is essential[27]. While making renewable energy consumption sustainable and acceptable to other developmental social-economic aspects, several criteria must be taken into account [29]:

- Ensure environmental sustainability by appropriately managing resources.
- Ensure a sustainable economy through developed infrastructure and services that maintain firm and stable affordability because of the disadvantaged rural population.
- Ensuring a stable and sustainable social sector that favours the poor, the children, the women and provides legal rights for all.
- Ensuring an active and sustainable administrative wing that can take up programs and implement them.

In conclusion, renewable energies, if effectively harnessed, have the potential to significantly reduce Africa's high energy demand and enhance rural areas' currently limited access to energy.

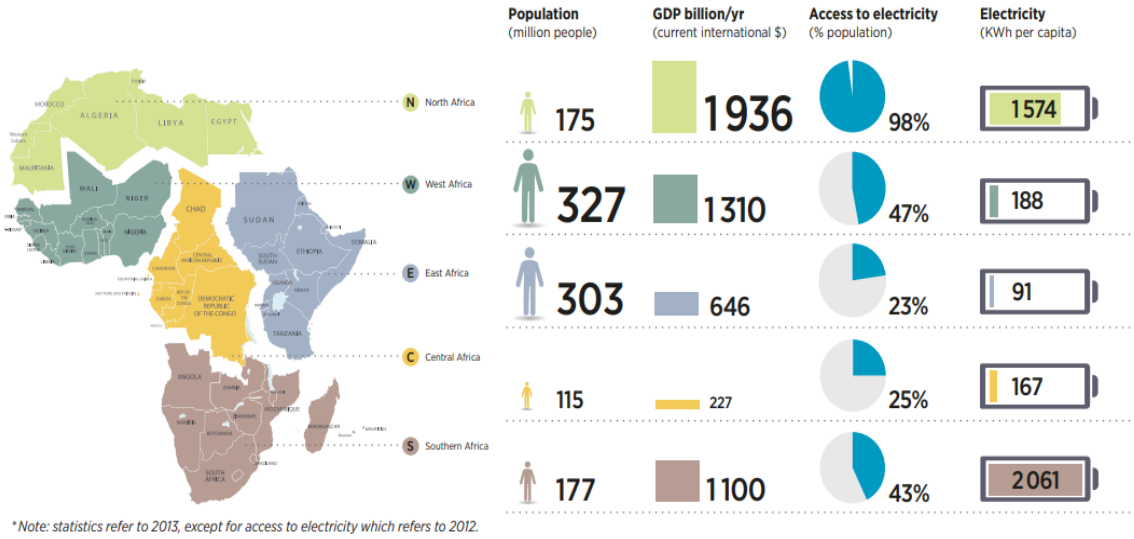

Figure 2.3: Africa's energy landscape[1].

2.2 Solar energy: source, resources, and possible deployment

The Sun, located at the centre of the solar system, is a self-gravitating gaseous body consisting mainly of hydrogen. It is located on an average of $1.5x10^{11}$ m from the earth thus it is the earth's closest star[30]. In the Sun's interior occurs fusion reactions that release energy. By nature, as the sun shines, the total energy that the earth's surface absorbs, and the entire atmosphere is sufficient to satisfy the annual global energy demands. This energy is transported through successive convection, absorption, radiation, emission, and reradiation to the photosphere. The photosphere, which absorbs and emits a continuous spectrum of radiation is the source of most visible radiation reaching earth. The surface temperature of the photosphere is 5777 K, a value equivalent to the temperature of a blackbody radiating an equal amount of energy as the Sun. The effect of gravitational force at the inner core of the sun creates a pressure that generates nuclear fusion turning hydrogen into helium. In the

process, an abundant amount of electromagnetic radiation is generated from a portion of the sun's mass thus making it a dominant source of radiative energy in the solar system. In agrarian communities, the abundance of the Sun's energy, combined with its seasonal availability, has established natural boundaries to human existence, societal development, and expansion, influencing the change of seasons and the wheel of the year[31].

The direct use of the sun's energy for heating and power generation is a relatively recent development in history. At the beginning of the 17^{th} century, physicians made attempts to concentrate solar radiation and eventually make it perform mechanical work. This was evident by the first sun-fuelled steam engine proto-type constructed by a French physic Salomon de Caus, using concentrating lenses. These devices were accurately described as toys than usable machines not until the year 1861 when Augustin Mouchot, a French mathematics teacher made attempts to produce enough steam to drive a small engine[30].

Despite its abundance, only a small amount of solar energy is directly used for human consumption. Human activities are highly powered by fossil fuels. They account for around 80% to 85% of worldwide energy use. Fossil fuels are non-renewable, suffer depletion, and emit greenhouse gases such as CO_2, which disrupt the ecological balance and are thus hazardous to the ecosystem[31]. Numerous attempts have been made to use fossil fuels in an environmentally friendly manner. Because large volumes of space are required to store the emitted greenhouse gases, the use of fossil fuels along with carbon sequestration became an extremely difficult approach. Despite being a good option, the adaptation of fossil fuels along with nuclear power suffers a less feasibility advantage[32]. The adverse negative environmental impact of fossil fuels made raise for the adaptation of other primary sources of energy. With a need to curb the ever-rising rates of greenhouse gas emissions in the world, solar energy took attention due to its green nature amongst all other renewable energy sources. In recent years, commercial and domestic solar energy usage has risen and continues to rise. In less developed countries, however, there is high domestic use of solar energy than commercial use.

There are two types of technologies for solar power generation: solar photovoltaic (PV) and concentrated solar power (CSP). Solar photovoltaics can be used in a wide range

of applications, from home systems to large-scale power plants. In utility-scale projects in arid areas and high-temperature zones, concentrated solar power technology performs well.

Despite the increased solar power installation, the demand too still increases but it is believed that the solar power potential exceeds demand expectations[1]. In 2019, more than 200 GW of additional renewable power-producing capacity was installed, according to the Renewables Global Status report for the year 2020. By December 2020, total world production had also risen to 2,588 GW. According to Fig.2.4, 2019 installations are higher than 2018, sustaining an average annual growth rate of more than 8% in installed renewable power capacity since 2015. In 2019, an estimated 115 GW of solar PV capacity was added globally, reinforcing the technology's position as the world's leading source of new energy generation capacity. Solar PV accounted for 57% of renewable power capacity increases in the same year, followed by wind power (30%) and hydropower (8%), with bio-power, geothermal power, and concentrated solar thermal power accounting for the remaining 5%[33].

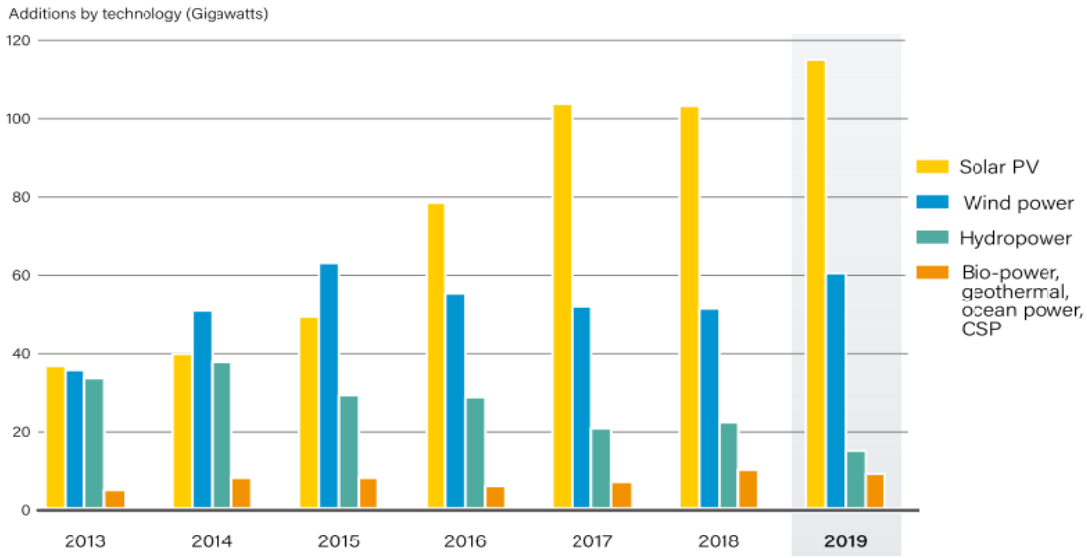

Figure 2.4: Annual Additions of Renewable Power Capacity[33].

Development partners such as the United Nations (UNs) and the World Bank are working on the Sustainable Electricity for All (SE4All) initiative in Africa, particularly in Sub-Saharan Africa, to offer sustainable and reliable energy by 2030. The role played by solar energy technologies in fulfilling the agenda of SE4All by providing a life-cycle basis

on a least-cost approach is under research. As a result, any program aiming at delivering off-grid energy locations had to achieve the basic service criteria aimed at fulfilling the SE4All. Off-grid solar PV technology, also known as stand-alone systems (energy systems that are not connected to a local, regional, or national grid), doubles the contribution to the SE4All goal and increases renewable energy access[18]. The ideal components of a domestic solar PV system for off-grid applications are presented in Fig.2.5.

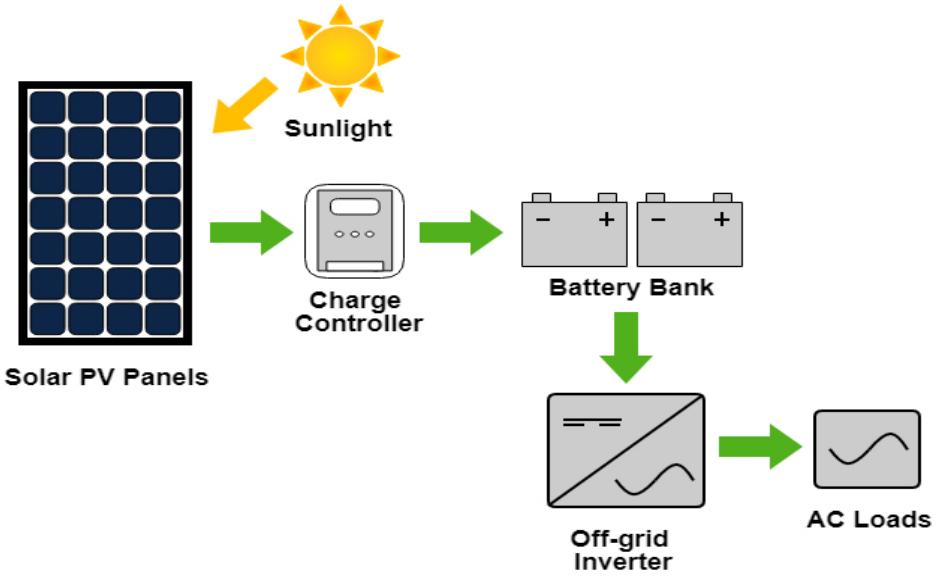

Figure 2.5: An off-grid solar PV system and its components[18].

Grid-connected systems, unlike off-grid systems, combine solar modules and grid-type inverters with a storage facility that eliminates costs on storage batteries. Grid-connected systems are typically deployed on rooftops of business buildings and parking garages to maximize space use. Grid-connected systems are constructed in such a way that when the PV produces more electricity than is required, the excess is put into the grid, while electricity is drawn from the grid when the PV produces less than is required. Since grid systems don't involve the use of batteries for storage, the system installation costs are relatively reduced[17], [18].

2.3 Wind energy

All over the world, countries are working on reducing the energy gap while mitigating the negative effects of energy utilization on climate change and the environment. In 2012, 19% of the global energy produced and consumed was from renewable energy sources while in 2013, production and thus consumption increased by 1%. Alternative to fossil fuels, wind energy has picked attention in the current global energy map. Researchers focus mainly on wind energy policy, technology development, and the role of wind energy usage on the control of environmental pollution and mitigate the emission of greenhouse gases thus reducing Global warming. Wind energy exists almost everywhere though the harvestable magnitudes exist in selected sites. International organizations and firms have strongly supported wing power resulting in a cumulative wind power capacity of 369,553 MW by the end of 2014 which is about a 16% increment past the installed capacity in 2013[34].

In the 90s, wind energy became the fastest growing renewable technology, per technology source compared to other energy production technologies in terms of annual installed capacity globally. In comparison to other technologies with inexpensive research and development costs, such as solar technology, wave energy, and fuel cells, the technology advanced rapidly into commercial application. It is worth noting that growth is still not uniformly distributed. By the end of 1999, over 70% of global wind energy capacity had been installed in Europe, 19% in North America, and 9% in Asia and the Pacific[35]. Research shows that in the near years, wind energy will be one of the highest produced and consumed renewable energy sources. In Africa, the theoretical wind power potential exceeds the demand by multiple times with more than 15% of the possible sources characterized to be high quality. Countries with good quality wind potentials include north African countries, Niger in the western part of the continent, Chad in the central, almost all the East African countries, and a few countries from Southern Africa including Malawi and Lesotho[1].

By the year 2018, about 51 GW of global capacity installed was realized registering a 4% decline from 2017(Fig.2.6). This includes about 47 GW onshore wind plants and about 4.5 GW offshore. Africa, Latin America Southeast Asia, and the Middle East accounted for a total of about 10% of the new installations, registering a 2% increment from 2017[36].

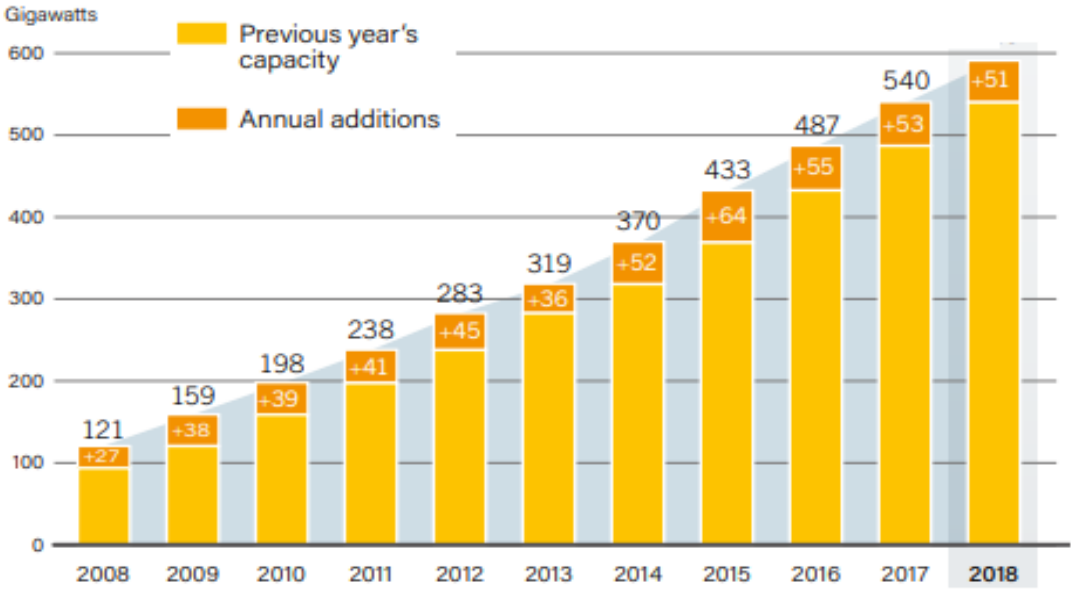

Figure 2.6: Installed wind energy capacity between 2008-2018[36]

2.4 Geothermal energy

Among the most renewable energy sources, the often ignored yet important is geothermal energy. This form of energy is present in both conventional hydrothermal and Engineered (Enhanced) Geothermal Systems (EGS). Geothermal energy resources are described as thermal energy content stored in the rock and fluids in Earth's interior that is accessible by mechanical processes such as drilling[37]. The origin of this thermal energy is associated with the earth's internal structure, chemical and physical processes that occur in the earth's crust. Heat present is unevenly distributed, not often concentrated, and in most cases present at depths that make their industrial exploitation almost impossible despite their existence in practically inexhaustible quantities. The natural movement of this heat from the earth's crust towards the surface is unnoticeable [38].

Since 1913, geothermal energy has been used to generate commercial power. In the last three decades, the use of geothermal energy has skyrocketed. By the year 2000, over 80 countries had recognized the energy source, with roughly 54 countries harvesting power from

geothermal energy and some utilizing it in its natural form. Global geothermal energy use is estimated to be 53 TWh/year for direct usage and 49 TWh/year for power and related applications, with geothermal steam accounting for the majority of this [39].

In Uganda, research, and exploration about the existence of geothermal energy has been going on since 1993. The areas of Buranga, Kibiro, and Katwe are in the final stages of surface exploration aiming at power generation from geothermal sources. Direct usage of the energy sources is yet to be documented, but the pilot study shows that subterranean temperatures are adequate for low-capacity electricity generation and direct usage[40].

2.5 Biomass energy

Biomass accounts for over 14% of global energy, with hydroelectricity accounting for 6%. In most developing countries, it is the most extensively used energy source, providing over 90% of total energy requirements in rural areas and serving as a major fuel source in urban areas and for many small-scale industries in both cities and suburbs. USA and Sweden obtain 4% and 14% of their generated power from biogas respectively despite the plan for further increase in bioenergy generation and use.

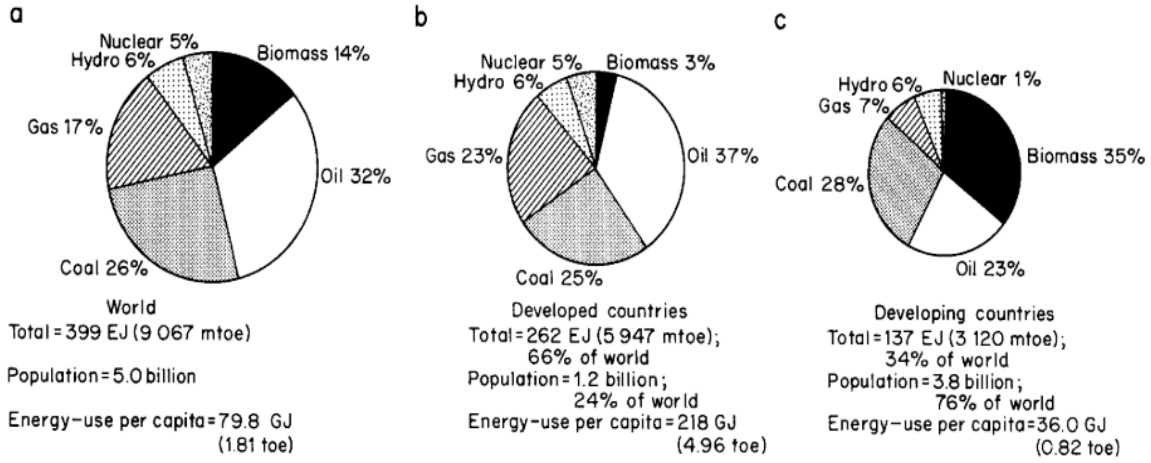

Figure 2.7: Global renewable energy use[42].

Despite the increased use of biogas energy, hardships in its transportation to the final consumers in an economical and environmentally friendly manner are increasing too[41]. In

percentage consumption, biomass contributes 14% to the global energy consumption with oil, coal, gas, hydro, and nuclear at 32%, 26%,17%,6%, and 5% respectively (Fig.2.7). It is estimated that the annual global biomass is 146 billion metric tons and production dominated by wild plant growth. About 35% of the energy consumed in developing countries is purely biomass. This raises the world's total consumption to be 14%. The future of biomass providing cost-effective and sustainable energy is promising[41].

CHAPTER 3

THE SOLAR CELL

Since the discovery of the first photovoltaic effect, the operational principle of a solar cell in 1839 by a French physicist, Edmond Becquerel, son of physicist Antoine Cesar Becquerel, solar energy utilization has been a global scientific objective[13]. Photovoltaic technologies stand advantages of being small and highly modular and thus applied in vast applications, unlike other electricity-producing technologies. The efficiency of the modules, the efficiency of the cells, and the meteorological conditions all influence the quantity of energy produced by a solar power plant[43]. This study focuses on the efficiency of solar cells. The total module's efficiency differs from the cell's efficiency. The difference is that panel efficiency is a composite value and generally smaller than the cells' efficiency because is affected by great energy losses in connectors and cables.

3.1 Solar cell and solar spectrum

Solar cells absorb a range of energy that corresponds to the solar radiation spectrum while in operation. The solar radiation spectrum comprises three major bands: the ultraviolet, visible (Photosynthetically Active Radiation, PAR), and infrared radiations. Of solar radiations reaching the earth's surface, 49.4% makes up the infrared radiation, about 8% constitutes ultraviolet radiation while 43.3% is visible light. Though solar radiation ranges between 100nm to 1mm wavelength as shown in Fig.3.1, most of radiation occurs between 250nm to 2500nm and in a visible light region of 400nm to 700nm for an air mass of Zero (0). As a result, solar cells must absorb as much energy as possible in the visible spectrum of solar radiation[13].

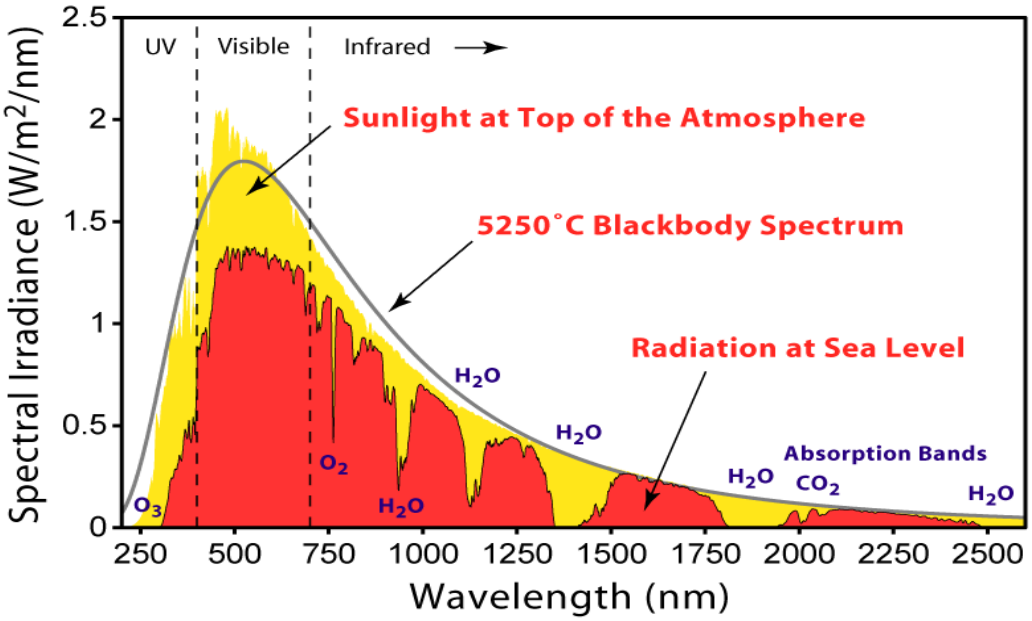

Figure 3.1: Solar insolation spectrum [13].

3.2 Generations of the solar cell

3.2.1 First-generation PV technologies.

Crystallized silicon cells are the first generation of PV technology. They are also referred to as silicon wafer-based solar cells. They were first developed in April 1954 by a group of researchers from Bell Laboratories in Murray Hill, New Jersey. In the year 1953, Daryl Chapin, a magnetic materials engineer was trying to develop an alternative power source for telephone systems following the rapid degradation of dry cell batteries. He discovered that solar power was the most promising one although his attempt was made with selenium solar cells which were less efficient. Later, researchers Calvin Fuller and Gerald Pearson who by then were researching on semiconductors discovered that current is created when a PN junction is created on Silicon. The three scientists combined efforts to develop a silicon solar cell. These cells were of 6% efficiency[13]. Currently, silicon-made solar cells occupy over 80% of the applications in solar panels around the world. This is attributed to the abundance of silicon, second to oxygen on earth. Silicon is a semiconductor with a 1.12 electron volt energy bandgap. In single-cell photovoltaic devices, silicon cells have a high-

efficiency level. The way silicon wafers are manufactured and the type of silicon employed determine how crystalline silicon cells are classified[44]. They are three types: Polycrystalline (Poly c-Si), Monocrystalline (Mono c-Si), and multi-crystalline silicon (mc-Si).

3.2.1.1 Monocrystalline (Mono c-Si) solar cells.

Despite being the earliest solar cell technology, monocrystalline solar cells are still the most popular and efficient solar cells. Their efficiency increases to 26% [44]. They are made of pure silicon with continuous crystal lattices. They are made from thin wafers of silicon by a process called Czochralski. Because they are carved from cylindrical ingots, they do not completely cover the module. The production of mono c-Si modules waves as early as 1963 by the Japanese-based Sharp Corporation.

3.2.1.2 Polycrystalline silicon or multi-crystalline silicon solar cells.

Polycrystalline silicon and amorphous silicon solar cells are less expensive as compared to monocrystalline silicon solar cells. This is mainly because of their manufacturing process and low levels of efficiency. Their efficiency goes up to 10%[45] although in some circumstances an efficiency of 21% is recorded[44]. They are manufactured from cast square silicon ingots.

All silicon solar cells contain two layers: a positive (p-type) and a negative (n-type) layer. The positive layer is made up of extra holes formed by boron doping, whereas the negative layer is made up of additional electrons in the silicon lattice formed by phosphorus doping. A PN junction is produced when these layers come into contact[11]. As radiation strikes the generated electrons, they gain photon energy allowing them to travel freely. However, because this movement is random, no current passes through the load. A driving force is required to make electrons flow unidirectionally[11][12]. In practice, a PN junction is a simple way to generate this driving force. When incident radiation reaches the N region of a PV cell's PN Junction, it penetrates and reaches the depletion zone, which is devoid of free electrons and holes. In the depletion area, this photon energy is sufficient to form electron-hole pairs. Electrons and holes are driven out of the depletion area by an electric

field. The concentration of electrons in the N region and that of holes in the P region reaches such a high level that a potential difference develops between them. When a load is connected across them, electrons flow as photocurrent through the load. Fig.3.2 describes the working principle of the silicon solar cell.

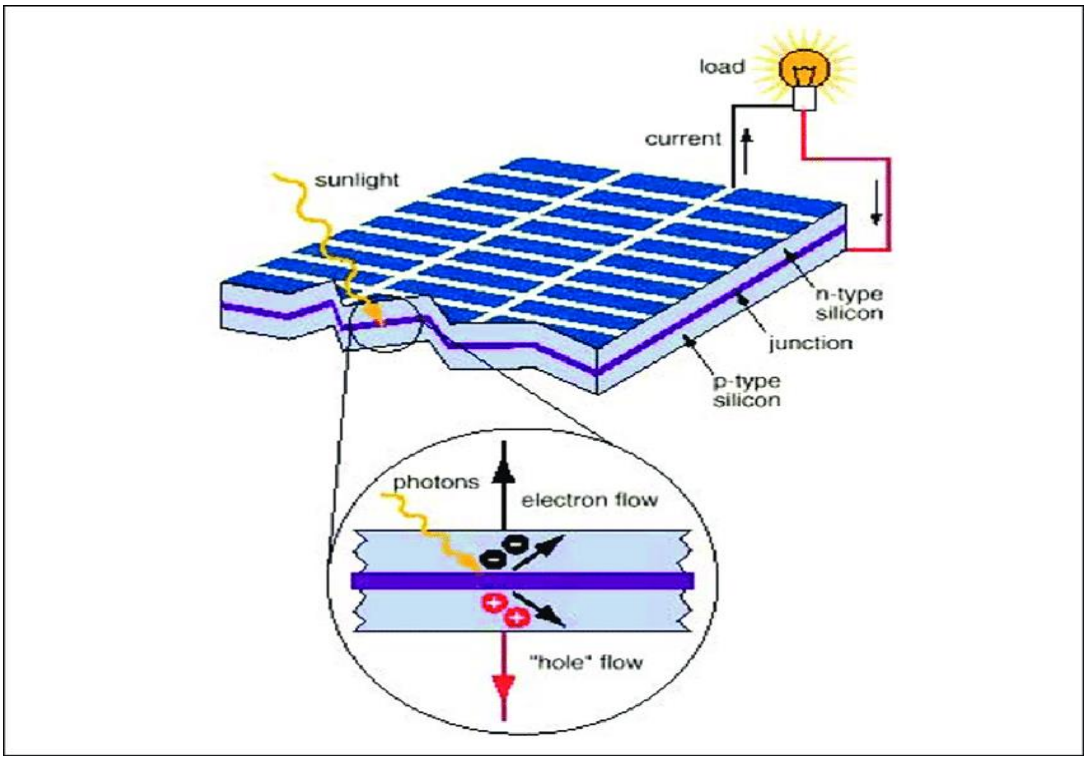

Figure 3.2: Silicon solar cell structure[13].

3.2.2 Second-generation PV technologies.

To curb the high cost of solar cell production, the need to switch from the “first generation” to “second generation” PV technologies became inevitable. The second generation PV technologies are known as the thin-film cell technology consisting of a combination of thin (between 1 to 4 μm thick) films of photon-absorbers and layers of stacks of the thin film [32]. They emerge by eliminating the Silicon wafer. In so doing, an appreciable reduction in material cost has been attained. The efficiency of thin-film solar cells is generally lower compared to wafer-based silicon solar cells, but they bear an advantage of lower production costs. Because of their thin nature, they can be easily

integrated into buildings (building-integrated PV, BIPV). The efficiency of the solar cell is dependent on the rate of incident solar radiation absorption, the rate of electron and hole collection, the order of the built-in potential, and the internal system resistance[46]. The following are the most common materials used in second-generation solar cells:

- Copper-Indium-Selenide (CIS)
- Copper-Indium-Gallium-Diselenide (CIGS)
- Cadmium telluride (Cd-Te)
- Amorphous silicon (a-Si) and micromorphous silicon (μc-Si).

In previous years, these accounted for roughly 20% of total panels on the market.

3.2.2.1 Cadmium telluride Solar Cells

They convert incident sunlight into energy with a maximum efficiency of 21.4 percent using a cadmium telluride semiconductor thin film. These cells cost 30% less than the Copper-Indium-Gallium-Diselenide cells and 40% less than amorphous silicon[45]. Care should be taken when using these cells as the cadmium, present in the cells is a toxic substance once release.

3.2.2.2 Amorphous silicon (a-Si) solar cells

They are made of amorphous silicon or micromorphous silicon. It comprises a PN junction as the basic electronic structure. They find applications in small electronic device such as calculators. Amorphous silicon cells, unlike other varieties, are created by depositing thin layers of silicon onto a backing metal, glass, or plastic substrate. Thin layers of silicon make the panels so flexible and of low cost. They suffer a disadvantage of very low efficiencies per unit area. Their efficiencies go up to 12%[13]. Complete absorption of radiation is made possible by making the layers thin enough since the amorphous structure has a lighter radiation absorption rate. The high inherent disorders and the dangling bonds of the amorphous silicon make it a bad charge carrier conductor. With a bandgap of 1.7eV more than crystalline Silicon (whose bandgap 1.1 eV), amorphous silicon absorbs visible light more strongly than the infrared radiation in the solar spectrum[45].

3.2.2.3 Copper indium gallium selenide (CIGS)

This is a semiconductor material with a tetrahedron bond and chalcopyrite crystal structure. It exhibits highest efficiency of about 2 21.6% amongst all thin-film materials[13]. Despite their low cost of production, all these thin-film solar cells have some drawbacks. Among the drawbacks are the high material costs (indium) and toxicity of cadmium. Because of these flaws, there was a demand for a new generation of solar cells.

3.2.3 Third-generation PV technologies.

Because of the poor electrical performance of thin-film technologies and high production costs of indium and toxicity of cadmium researchers emerged with third-generation PV technologies. This category of solar cells is quite different from other solar PV generation as it does not use a PN junction. Besides silicon, the new generation of solar cells employs materials such as Silicon wires, nanomaterials, organic dyes, conductive plastic materials, and solar inks[45]. The main aims of the third-generation solar technologies are to provide an efficient energy consumption means for a wide band, avail solar energy to consumers at a relatively cheaper cost, making solar consumption less toxic, and lastly, provide a vast use of solar energy. This generation employs various innovations in solar energy including but not limited to nanocrystalline cells, polymer, and dye-sensitized solar cells.

3.2.3.1 Organic and polymer solar cells

Conducting polymers became a new class of materials after their discovery and developments in recent years by three chemists: MacDiarmid, Heeger, and Shirakawa. Their structure is based on SP^2- hybridized (one S-orbital and two P orbitals of the free atom) carbon atoms[47]. The application of a semiconducting conjugated polymer to a thin film photovoltaic device creates a polymer solar cell. Polymer solar cells have a highly delocalized π-electron that enables both absorptions within the visible light region and electrical charge transport. Polymer solar cells have improved power conversion efficiency from 3% to around 9% in recent solar energy breakthroughs[48]. Solution-processing

techniques are used to create polymer solar cells with low-cost energy collecting advantages. Flexible solar modules, architectural applications (semi-transparent solar cells in windows), and liquid-crystal displays all use these cells.

The operation mechanism of polymer solar cells is presented in Fig.3.3. The active region of this Cell consists of an electron donor material and an acceptor. Charges remain bound in the form of an exciton when a photon of light is transformed into a pair of electrons and holes in the donor material. The difference in energy between the donor's lowest unoccupied molecular orbital (LUMO) and the acceptor's highest occupied molecular orbital (HOMO) provides excitons with a driving force (effective field). The excitons are broken up by effective fields formed by the heterojunction between two different materials, and an electron falls from the donor's conduction band to the acceptor's conduction band[13], [45], [48].

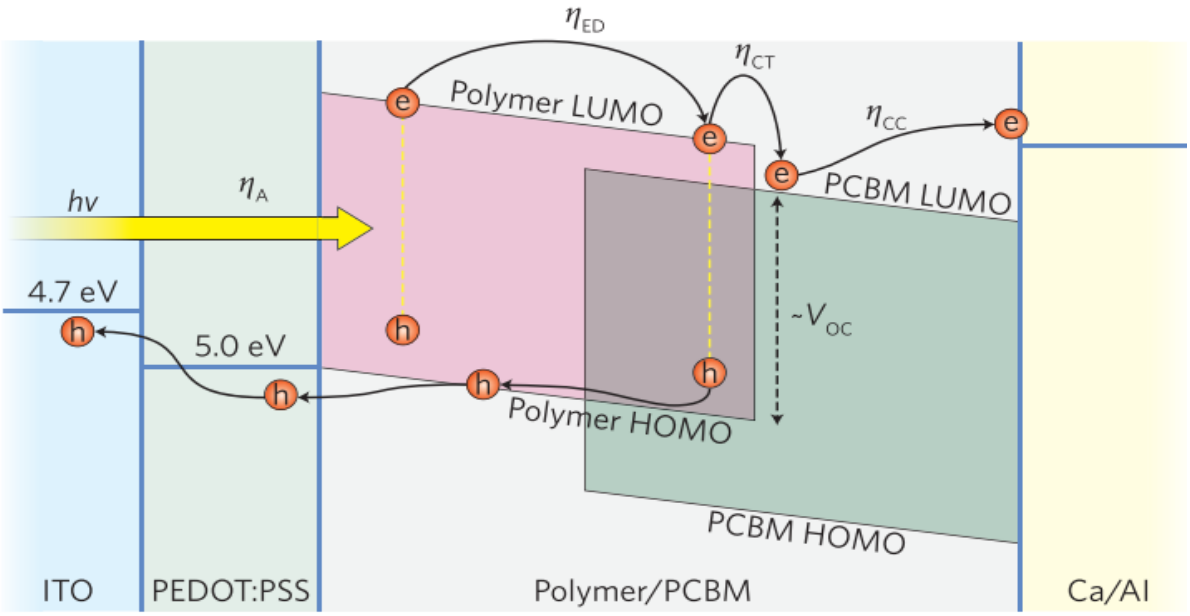

Figure 3.3: The operating mechanism of a Polymer solar cell[48].

The electrons and holes are eventually gathered onto the cathode and anode, respectively, after separation. The efficiency of polymer solar cells is limited by the short exciton diffusion length.

3.2.3.2 Quantum dot solar cells (QDSCs)

They are either self-assembled quantum dots (SAQDs) or colloidal quantum dots (CQDs). These cells fall in the same category as the dye-sensitized solar cell. The only difference is that they employ low bandgap semiconductor nanoparticles to absorb light other than organic and organometallic dyes. The low bandgap semiconductor nanoparticles are known as quantum[49].

3.2.3.3 A dye-sensitized solar cell (DSSC, DSC, or DYSC)

They are commonly known as Grätzel cells; a name that originates from their inventor, Michael Grätzel in 1988 at the University of California. DSSCs have several advantages over other solar cells, including comparatively high efficiency, somewhat low cost and simple fabrication techniques, environmental friendliness, and good flexibility. The composition of the dye, surface structure, grain size, and photo-electrode thickness of TiO2 all affect the performance of these cells. Despite their detrimental effects on solar cells, such as short-term dye stability due to evaporation and leakage, using liquid electrolytes in solar cells enhances overall conversion efficiency by 12 percent or more [13]. Photons are absorbed by a sensitizer mounted on the surface of a wideband semiconductor in DSSC, and electron transfer or transport happens at the interface by photo-induced electron injection into the solid's conduction band from the dye. This method distinguishes DSSC from traditional PV systems. An illustration of DSSC is shown in Fig.3.4. It is made up of a porous layer of titanium dioxide (TiO_2) nanoparticles that act as the anode, and a light-absorbing molecular dye on top. TiO_2 is totally immersed in an electrolyte solution, above which is attached a platinum catalyst that acts as a cathode. The anode and cathode thus appear on either side of the electrolyte solution. Sunlight striking the solar cell passes through the transparent electrode into the dye layer. The electrons in the dye are excited and flow into TiO_2.

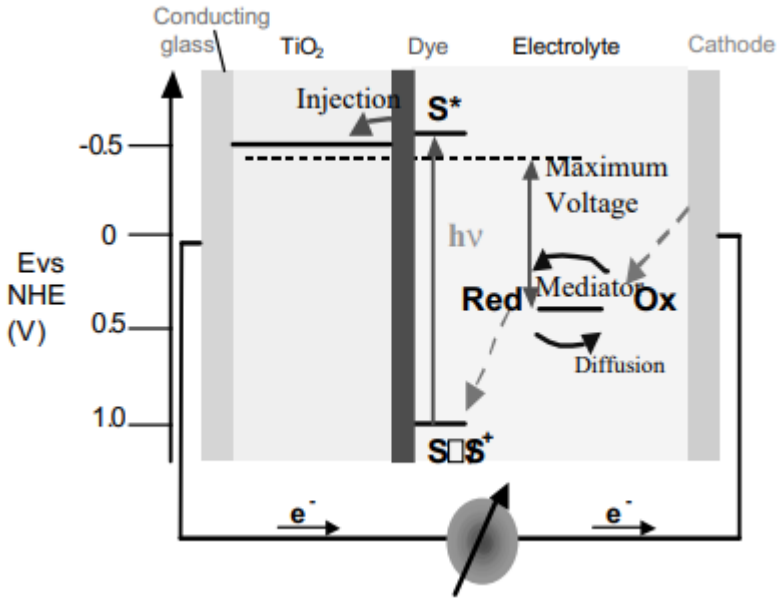

Figure 3.4:A dye-sensitized solar cell[50].

Electrons are then collected at the transparent electrode to power the load. Electrons are introduced again into the circuit after passing through the external circuit and they flow back into the electrolyte[13], [45], [50].

3.3 Working principle of a solar cell

PV cells are made up of wafers, which are tiny silicon slices that make up the heart of the photovoltaic cell[11]. Because silicon atoms are bound together, electrons in the silicon structure have no freedom of movement. Photon energy is transmitted to the silicon atoms when light strikes the N-P diode. The energized atoms from the p-type layer cross the depletion region, generating pairs of electrons and holes across the whole device. When the system is open-circuited, the depletion region is reduced. The reduction is brought about by electron-hole pairs formed at a region in the neighbourhood to the depletion region, which recombines with the charge in this region. Eventually, the charge in this region reduces resulting in a potential drop across the device open terminals. Theoretically, the maximum voltage (open circuit voltage) is developed when the depletion region is eliminated, as presented at point C in Fig.3.5. This phenomenon is impractical in real-life operations.

When the terminals are closed, generated electron-hole pairs result in a current, equivalent to the photon of light striking the cell's surface. This is the short circuit current. The short circuit current corresponds to point A in Fig.3.5.

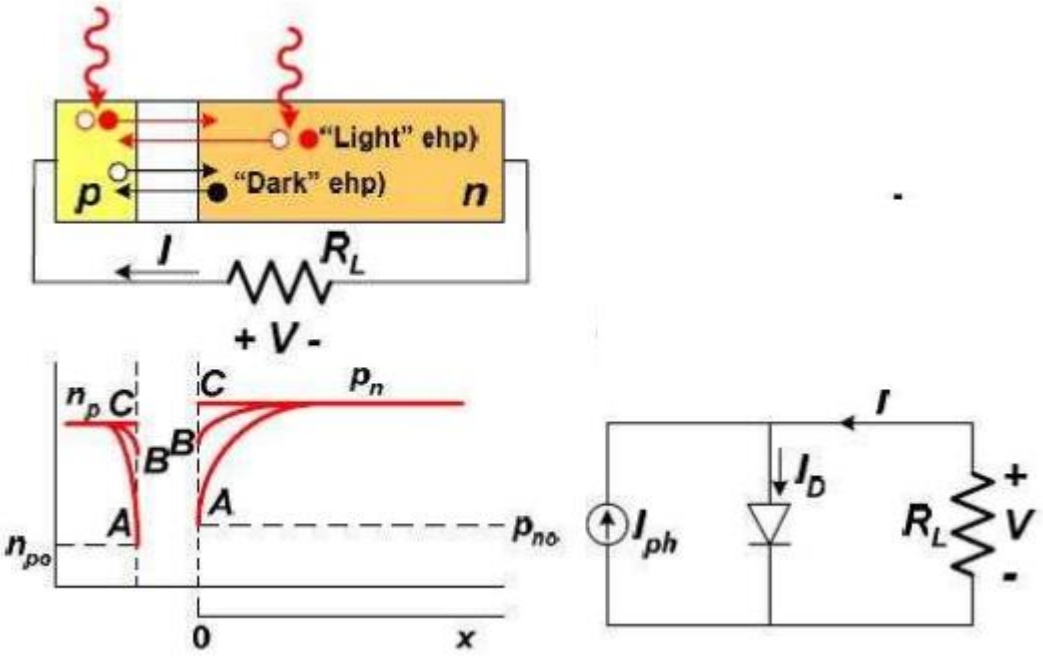

Figure 3.5: Working principle of a p-n diode solar cell[32].

The device only operates in the region between points A and C when the load, say R_l, is connected across the terminals. This is because of the voltage drop across the resistor (Load) keeping the device's maximum voltage always less than the open-circuit voltage[32]. While in operation, the device is forward biased and this generates a current called the dark current, that flows in the direction opposite to that of current generated by the photons. As a result of this dark current, the device does not operate at short-circuit current. This proves the fact that a solar cell only generates power using the light radiation incident on its surfaces.

3.4 Solar cell efficiency limits

The utmost single-junction solar cell theoretical conversion efficiency limit under one sun is estimated to be 31%. This limit is known as the Schokley-Quiesser limit. When the

solar cells are exposed to high-intensity sunlight i.e., 50,000 suns, the maximum efficiency of single-junction solar cells increases by approximately 10% as illustrated in Table 3.1.

Table 3.1: Future efficiency improvements across device configuration [31]

Approximate Theoretical limit Efficiency		Approximate Best experimental performance to Date	
Thermodynamic (concentrator)	87%	n/a	
Thermodynamic (1 sun)	68%	n/a	
Six-Junction	58%	n/a	
Hot carrier	54%	n/a	
Triple-junction concentrator	64%	44%	III-V alloys, monolithic stack
Triple-junction (1sun)	49%	15%	Thin-film amorphous silicon alloys
Double-junction concentrator	56%	30%	III-V alloys, monolithic stack
Double junction (1sun)	43%	12%	Thin-film amorphous silicon alloys
Shockley-Queisser single-junction (46,200 suns)	41%	30%	Crystalline silicon (500 suns)
Shockley-Queisser single-junction (1 sun)	31%	24%	Crystalline silicon
		20%	Thin multi-crystalline silicon
		12%	Dye-sensitized cell
		6%	Organic cell

These performance efficiencies can be modified further through junction coupling. The formation of multi-junction solar cells enables more energy from the solar spectrum to be trapped. The approximate theoretic thermodynamic PV efficiency limit with one sun is 68% and can be increased by 19% with adequate solar concentration[32].

3.5 Solar cell cooling technologies

3.5.1 Effect of cell temperature on performance.

When solar radiation reaches the surface of the PV module, a large portion of the absorbed solar radiation is dissipated as heat. This heat raises temperature of the cell, reducing electrical output and efficiency[51]. PV cell conversion efficiency is directly related

to temperature as seen from Fig.3.6[52]. Figure 3.6 shows that conversion efficiency varies inversely proportional to the PV cell surface temperature. Short circuit current (I_{sc}) directly varies with temperature while open-circuit voltage (V_{oc}) and maximum power (P_{max}) as efficiency, exhibits an inverse relationship.

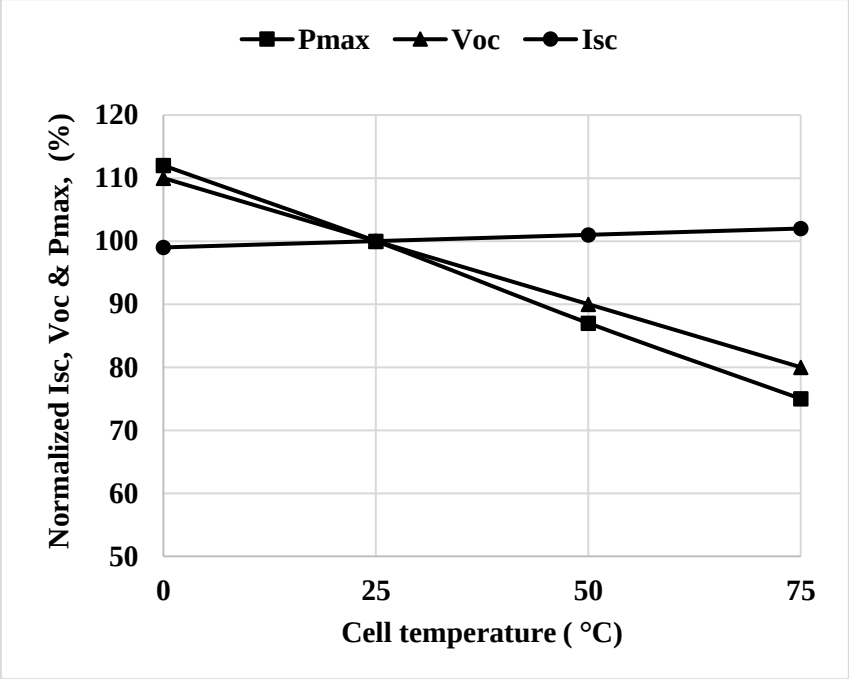

Figure 3.6:The influence of temperature on the conversion efficiency[52].

From Fig. 3.6, it is evident that a solar cell operates at maximum output at surface temperatures equal to or less than 25ºC. To keep the PV cell at the proper temperature limit, various strategies have been used. Solar power generation technique applied, and the meteorological circumstances of the installation location are some of the factors to be considered when designing an effective cooling system. Passive and active cooling techniques, as well as the combination, are used in PV solar thermal control.

3.5.2 Passive cooling technologies

Passive cooling is primarily used to cool PV cells that do not have concentrators or that have concentrators that are up to 10 suns[53][54]. To successfully boost heat dissipation, almost all passive cooling solutions necessitate the addition of extra components to the

system. This extra component can be either a heat pipe or a heatsink. Passively cooled PV systems have a low balance of system cost but exhibit low-performance efficiencies. Passive cooling mainly involves two approaches i.e., incorporation of heatsinks and using a heat spreader (heat dissipation plate). In the latter approach, a metal plate is used to evenly spread heat from sunlight before concentration on the cell [55] as shown in Fig.3.7. In such a system, the total energy received by the module and that received by the flat pate is the same, but the cell temperatures could be lowered to as far as the flat plate temperature. Flat plates can be made from one of the following categories of materials: Pure metals, Alloy category, Ceramics category, and Diamond categories[56].

The use of heatsinks as a thermal management tool is affiliated with their simplicity in nature, ease of maintenance, and low installation and operating cost[57]. However, problems of high heat fluxes, compactness, and increased power in the different electronic devices make the associated heat transfer more complicated.

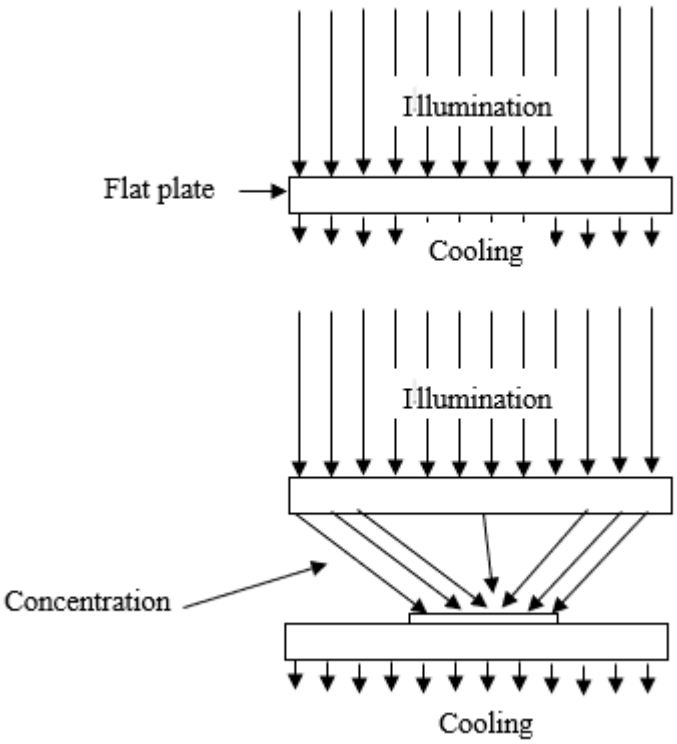

Figure 3.7:Concept of heat spreading in concentrated PV solar systems[55].

The use of heat sinks as one of the heat dissipation enhancement is among the best technologies. Heat sinks operate on Fourier's law of heat transfer i.e. whenever a temperature gradient exists, heat transfer occurs in a direction of reducing temperature[58]. Heat sinks are either air or liquid cooled[59]. In present field applications, air-cooled heatsinks could not meet the demand and thus, liquid-cooled heatsinks are more preferred. Liquid-cooled heatsinks are channel heatsinks. Aside from channel geometry, the coolant type, volume flow rate, operating conditions, and heatsink material all play a role in the performance of a liquid-cooled microchannel heatsink. [60]. Water is mainly used as a coolant liquid despite its corrosive nature because of its abundance. In some applications, nanofluids are used. Air-cooled Heat sinks employ natural (passive) or forced (active) convection and sometimes both[61]. Heat pipes or thermal interface materials (TIM) are also applied in passive cooling though their application is limited to the type of the system.

3.5.3 Active cooling technologies

In active cooling, heat transfer fluids are used to effectively regulate temperature for high power density packed cells with the aid of an external device to efficiently enhance heat dissipation[53]. Active cooling can be conducted under two approaches: the open-loop or closed-loop approach. These approaches can also be used simultaneously. Mechanical or electrical components, such as pumps and fans, are used in all active cooling technologies. This means that active cooling techniques require additional external power to operate. The benefits and drawbacks of various PV thermal management techniques are extensively discussed by A. Hasan et al [62]. A conclusive study on these advantages and disadvantages is helpful for the selection of the best approach.

3.6 Thermal regulation enhancement by phase change materials, PCM

Phase-changing materials are applied in both latent and sensible heat storage systems. Manish K.2008 [63] categorizes them as organics, inorganics, and a eutectic mixture of organic and inorganic materials. Fig.3.8 illustrates a tree diagram to classify PCMs. Inorganic

PCMs face the setback of phase separation. This occurs because of incongruent melting and variation in densities of inorganic salts and water. Phase separation can be eliminated by mechanical stirring, PCM encapsulation, use of gelling agents, extra-water principle and property modification.

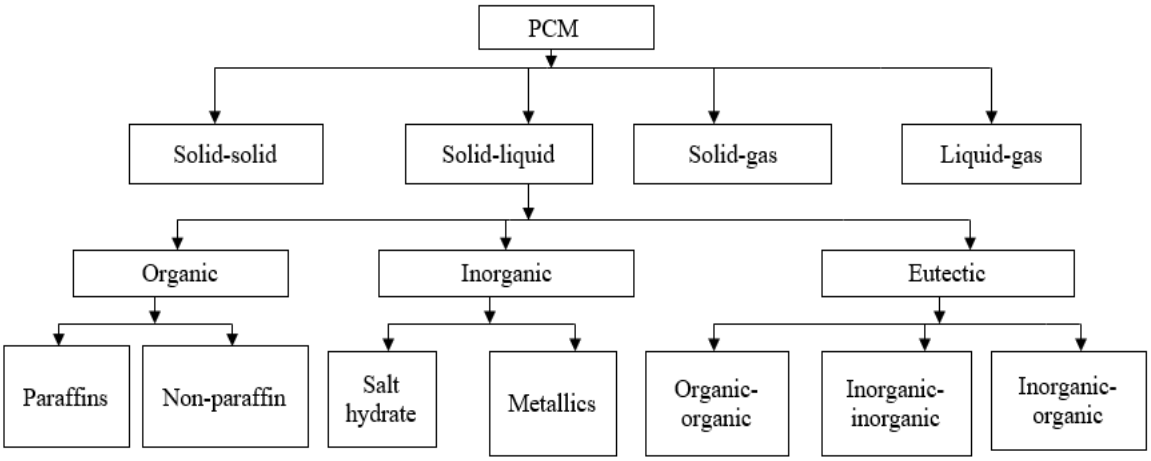

Figure 3.8: PCM classification[63].

In addition to phase separation, most phase change materials face problems of super-cooling or sub-cooling, low thermal conductivity, poor thermal stability, and corrosion. Kavendra et al [64] explain the remedies to the above problems.

As the PCM temperature raises to its melting point, sensible heat is absorbed. This energy is dependent on the PCM mass, m, its heat storage capacity C_p and the magnitude of temperature change[19]. Sensible energy stored or released Q can be expressed analytically by Eq. (1.1).

$$Q_s = mc_p \int_{T_1}^{T_2} \Delta T = mC_p(T_m - T_i) \qquad (1.1)$$

T_1 and T_2 are the initial and final operating temperature levels of the systems.

Latent heat is absorbed or released during melting since it involves the material's phase transition. Energy storage or release occurs as a result of enthalpy change as the material changes its phase[19]. The amount of Latent energy stored or released, Q depends on the mass, m of the PCM and its latent heat of fusion L and is expressed as in Eq. (1.2).

$$Q_l = mL \tag{1.2}$$

An appreciable amount of further sensible heat is absorbed from the point when the PCM is fully molten up to when it attains peak equilibrium temperature [62]. A combination of these energies constitutes the total heat absorbed or released by the PCM while in operation. This can be expressed by Eq. (1.3). Fig.3.9. illustrates the energy changes as the PCM changes its phase.

$$Q = m\{C_{ps}(T_m - T_i) + L + C_{pl}(T_F - T_m)\} \tag{1.3}$$

PCM application goes as far as energy storage in buildings with no or minimal mass enhancement. As phase transition occurs, PCMs absorb a significant quantity of thermal energy depending on storage capacities. The stored heat will be released once the liquid PCM solidifies[65]. Because energy stored in PCM is latent, the release and absorption of heat occur with only minor variations in the material's temperature, as opposed to sensible heat storage.

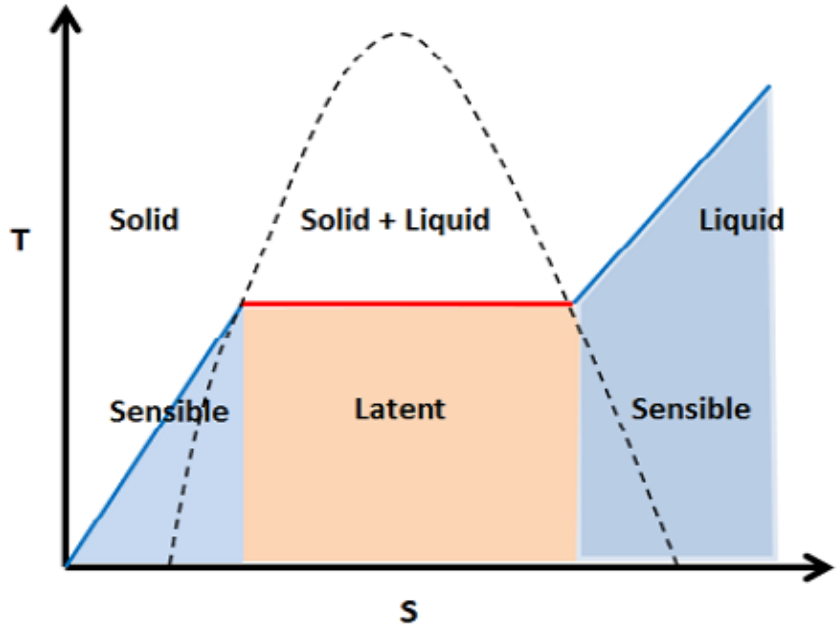

Figure 3.9:Heat storage principle of PCM [70].

Latent heat storage (LHS) is preferred over sensible heat storage (SHS) because of the ability to store large energy density, system compactness, and uniform storage temperature[66].

PCMs exhibit various melting temperature ranges depending on their properties. Factors for the choice of the PCM materials are not only limited to its properties but also its storage capacity, operating temperatures, heat transfer fluid, and system design[67] [68]. For latent heat storage (LHS) applications, molten salts are highly preferred over molten metal alloys[66]. In high-temperature energy storage systems, molten metals outperform molten salts. This is because of their excellent thermal conductivity. This accounts for their application in nuclear power reactors[66]. In solar steam power systems with temperatures ranging from 200 to 600°C, inorganic salts such as $NaNO_2$, $NaNO_3$, KNO_3 are used as energy storage systems. Inorganic salts may be pure substances or eutectic mixtures[69].

In literature, several studies about thermal management in photovoltaics by natural convection, forced convection, liquid cooling, and cooling by phase-changing materials have been conducted either numerically or experimentally.

H.A. Nasef et al[53] investigated thermal regulation in concentrated photovoltaic cells with active cooling technologies using PCM, water, and a nanofluid. According to the results of the numerical analysis, using a nanofluid as a heat transfer fluid reduces temperature by 60% compared to using a PCM with water cooling systems. Results further reveal that the use of nanofluid as compared to water results in an efficiency increase of 2.7%, lowers the temperature by 4 °C, and reduces PCM melting time by 12%. Similar studies were presented by AL-Musawi et al 2019[21] and Sardarabadi et al. 2017[70]. For both authors, the use of PCM together with a nanofluid exhibited a better thermal regulation than the use of water.

Huang et al. 2011[71] experimented on thermal management of an internally finned phase-changing material in photovoltaics. He investigated the effects of PCM crystalline segregation on heat transport inside various configurations of PV/PCM coupled with internal metal fins. The study concluded that PCM usage passively limits the PV temperature rise. Fins improve efficiency though the system's weight limits the size and the number of fins used.

Manikandan et al. 2019[72] presented a numerical analysis on solar thermal management with a heat sink and PCM. A layer of PCM domain was introduced on the

backside of the CPV module to keep the surface temperature lower than the ambient temperature. Results show that the addition of a PCM showed significant thermal management compared to a conventional CPV without a PCM also with a fin height increment from 0.75mm to 3mm, temperature lowered by 23°C from 55°C. This resulted in increased efficiency and power.

Ideally, successful utilization of a phase change material in energy storage or thermal regulation system depends entirely on the selected PCM visa vie the nature of the application. The choice of the best PCM for a given application depends mainly on its thermal physical properties. Other considered properties include the chemical stability under a given heat transfer medium and the thermal behaviour of PCM with the selected cooling fluid.

3.6.1 Integrated PCM-Air cooling.

For effective use of a combined air-PCM cooling technique, a concise study on PCM properties is highly important. When the ambient air temperature, which ideally serves as the cooling air temperature is higher than or nearly equal to the PCM melting temperature, the integrated system is less effective or completely ineffective. This is because the ambient temperature will account for the melting of the PCM. In such a situation, the air must be cooled below the melting point of the PCM, before being directed into the cooling duct. To attain this, the ground heat exchanger, also known as the earth-to-air heat exchanger (EAHE) should be used. EAHE is a technique that is applied to preheat the air in winter conditions and to provide cold air in the summer seasons. It is mainly for thermal management in the building. Research shows that at a depth of 2 to 3 m below the surface of the earth, the temperature remains nearly uniform and constant throughout the entire year[73]. This uniform temperature, the earth's undisturbed temperature (EUT), is always lower than the surrounding temperature in summer and higher in winter seasons. In the operation of EAHE for summer application, hot inlet air from the ambient is passed through a series of vertical or horizontal pipes buried at a depth of 2 to 4m depending on the location. The inlet airflow is aided by a mechanical device such as a blower, fan, or pump[74]. Heat exchange between the pipe material and the surrounding soil domain occurs as the air blows through the pipe.

The region of the soil adjacent to the pipe of the EAHE that is affected by heat transfer is called the thermally disturbed soil layer. Its thickness varies, and the exact thickness is not known[75].

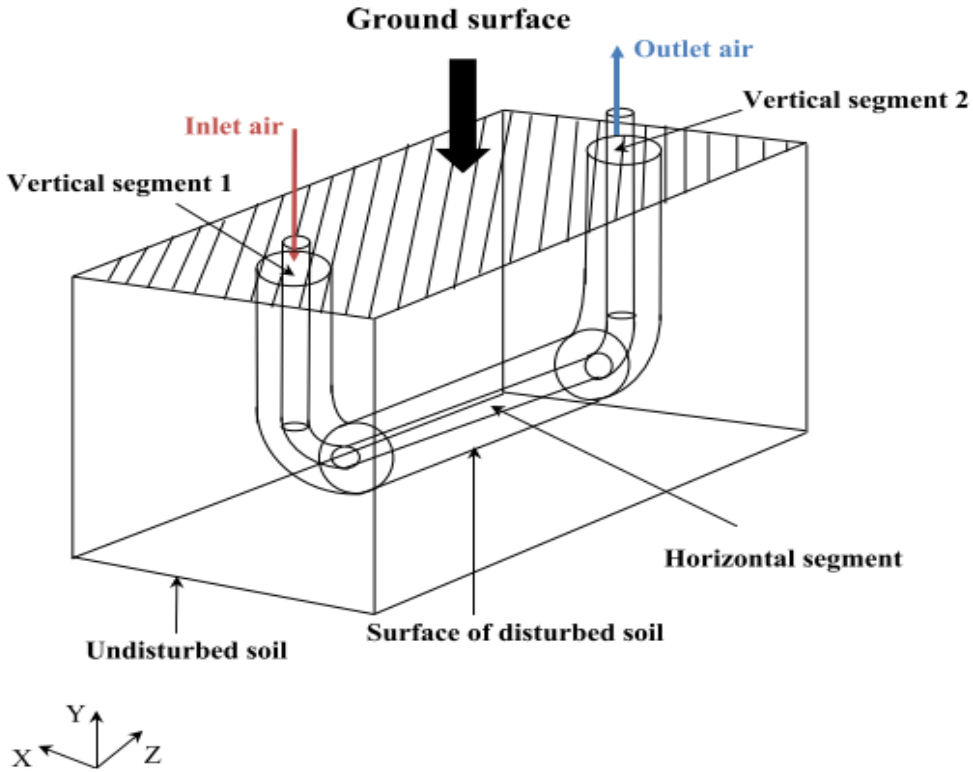

Figure 3.10:Principle of operation of EAHE [75].

When the interior air is re-circulated, the system is said to be a closed loop, otherwise, it is an open-loop system. Fig.3.10 shows a simple illustration of the principle of operation of the EAHE. Al-Ajmi et al[74] examined the cooling potential of the EAHE for a hot and arid climate of Kuwait by an analytical model. In their study, both the thicknesses of the disturbed soil layer and the radius of the pipe were assumed equal. The pipe was assumed to be of zero thermal resistance. TRNSYS environment simulation results revealed that the EAHE provides about 30% cooling in the summer season for lower inlet air velocity.

CHAPTER 4

NUMERICAL MODELLING

4.1 Material selection.

For this study, a 500 mm x 500mm small-scale monocrystalline photovoltaic module was presented. The PV panel considered is a layer of tempered glass, solar cells encapsulated between two layers of EVA and PVF layer respectively from the top surface[73]. The layers are enclosed within an aluminium enclosure. The transparent ethylene-vinyl acetate (EVA) lamination prevents humidity effects on the cells and prevents dirt from penetrating. EVA also helps cells withstand shocks and vibration because of wind as they float between the glass plate and the back sheet. Most modules possess a metal rear contact which provides mechanical strength, improves resistance to weathering, and provides electrical insulation of the cells[77]. The PVF too acts as insulation. Thermal properties of each layer of the module and those of the PCM are presented in Table 4.1. Properties of PV layers remain constant with variations in both temperature and pressure. In the numerical simulation, the PV module is treated as a single layer with thermal properties of PV cells[52]. An organic RT35 PCM whose melting range is close to the Standard Test Condition temperature was selected for this application. This type of PCM exhibits higher thermal storage capacity at an approximately constant temperature range[78].

4.2 Model Configurations

The study was conducted considering 4 PV module configurations as shown in Fig.4.1. These include PVT module, PVT/PCM-I, PVT/PCM-II, and PVT/PCM-III. The PV module is exposed to solar radiation of 540 W/m^2, the average hourly direct solar irradiation in Uganda[79], and an air film coefficient of 8 W/m^2 K with an ambient air temperature of

26ºC. With the same thermal conditions, a layer of RT35 PCM was introduced below the pannel in PVT/PCM-I.

Table 4.1: Material properties [76][53][80][81].

Component	Parameter	Value	Unit
Glass cover	Density,ρ_g	3000	kg/m^3
	Thickness, δ_g	0.003	m
	Specific heat, C_g	500	J/kgK
	Thermal conductivity, k_g	2	W/mK
	Emissivity, ε_g	0.9	-
	Absorptivity, α_g	0.04	-
	Transmissivity, τ_g	0.92	-
Silicon layer (PV cells)	Density,ρ_{sc}	2330	kg/m^3
	Thickness, δ_{sc}	0.0002	m
	Specific heat, C_{sc}	667	J/kgK
	Thermal conductivity, k_{sc}	148	W/mK
	Absorptivity, α_{sc}	0.9	-
	Packing factor, β_{sc}	0.9	-
	Temperature coefficient, $\beta_{1,ref}$	0.0045	K^{-1}
	Reference efficiency, η_{ref}	0.2	-
EVA	Density,ρ_e	960	kg/m^3
	Thickness, δ_e	0.0005	m
	Specific heat, C_e	2.090	J/kgK
	Thermal conductivity, k_e	0.35	W/mK
RT35 PCM	Thermal conductivity	0.2	W/m K
	Density (solid/liquid)	860/770	kg/m^3
	Specific heat capacity (solid/liquid)	1800/2400	J/kgK
	Latent heat	160,000	J/kg
	Viscosity	0.001798	kg/m^{-s}
	Melting area	302-309	K

The PCM is enclosed in an insulating material to ensure proper melting and solidification. The base of the PCM enclosure is expose to natural convection. In PVT/PCM-II, copper fins, whose material thermal conductivity, density, and specific heat capacity are 400W/mK, 8933 Kg/m^3, and 385 kJ/kgK[80] respectively were introduced to the PCM layer and subjected to the same thermal conditions. Fins are designed as a plate heat sink with a 2mm thick base, sides being equidimensional to the module. In PVT/PCM-III, a rectangular air duct is introduced below the entire surface of the PCM to further improve cooling.

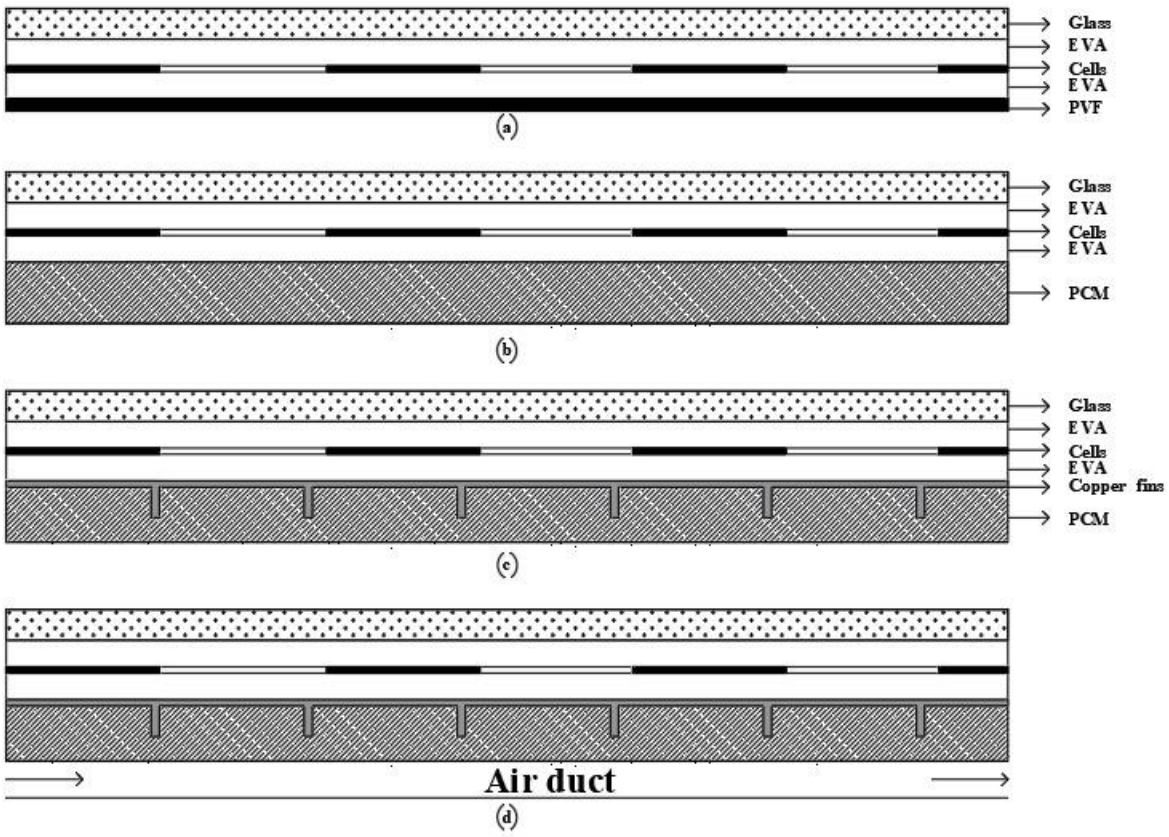

Figure 4.1: Schematic cross-section of a photovoltaic module system: (a) without cooling (PVT module), (b) PCM with insulation at the bottom (PVT/PCM-I), (c) PCM with copper inserts and insulated at the bottom (PVT/PCM-II), and (d) PCM with copper inserts and cooled by air flowing over the bottom surface of PCM (PVT/PCM-III).

4.3 Enthalpy-porosity formulation

The enthalpy-porosity approach was used to model phase-changing process. The energy balance is used as a foundation for calculating the liquid fraction in this method. The mushy zone, defined as an area with a liquid fraction between 0 to 1, is introduced and handled as a "pseudo" porous medium. The porosity is equal to the liquid fraction in the mushy zone and changes from 0 to 1 as the PCM melts[81]. The governing equations for the flow take the form below[20].

X-direction momentum equation.

$$\rho\left(\vec{V}\cdot\nabla u\right) = -\nabla P + \mu\nabla^2 u + S_x \tag{4.1}$$

Y-direction momentum equation.

$$\rho\left(\vec{V}\cdot\nabla v\right) = -\nabla P + \mu\nabla^2 v + S_y + F_b \tag{4.2}$$

Z-direction momentum equation.

$$\rho\left(\vec{V}\cdot\nabla w\right) = -\nabla P + \mu\nabla^2 w \tag{4.3}$$

In the above equations, $\nabla = \frac{\partial}{\partial \mathrm{x}} i + \frac{\partial}{\partial y} j$ and $\nabla^2 = \frac{\partial^2}{\partial \mathrm{x}^2} i + \frac{\partial^2}{\partial y^2} j$. F_b is buoyance force which is calculated from the Boussinesq approximation [82].

$$F_b = -\rho_o g(1 - \beta_1(T - T_o)) \tag{4.4}$$

In Eqn. (4.4), β_1 is the thermal expansion coefficient, ρ_{liquid} and T_m are the density and temperature respectively at the melting point. Terms s_x and s_y are Darcy's law momentum sink terms that cater for the reduced porosity in the partially solidified regions of the PCM[20], and they are calculated from Equations (4.5) and (4.6).

$$s_x = \frac{(1-\lambda)^2}{(\lambda^3+\gamma)} A_{mush}.u \tag{4.5}$$

$$s_y = \frac{(1-\lambda)^2}{(\lambda^3+\gamma)} A_{mush}.v \tag{4.6}$$

In equations (4.5) and (4.6), λ represents the fraction of the liquid PCM present in the PCM domain as it melts (liquid fraction) and γ, is a negligibly small numerical value about 0.001[82] introduced to eliminate errors resulting from division by zero. A_{mush} is a mushy zone constant. A_{mush} explains the steepness of the velocity as it reaches to zero when the material is undergoing solidification. The value of A_{mush}depends on the morphology of the phase-changing material and takes on numerical values between 10^3 and 10^8 kg/m^{3}s. For the current study, the value of A_{mush} is kept at 10^8 kg/m^{3}s for better prediction[20].

The energy equation for the phase changing material reduces to;

Liquid phase $$\frac{\partial}{\partial t}(\rho_l H) + \nabla \cdot (\rho_l \tilde{v} H) = \nabla \cdot (k_l \nabla T) + S \quad (4.7)$$

Solid-phase $$\frac{\partial}{\partial t}(\rho_s H) = \nabla \cdot (k_s \nabla T) \quad (4.8)$$

S is the source terms. PCM enthalpy, H, is the sum of the sensible enthalpy, h, and the latent heat ΔH, and calculated as follows:

$$H = h + \Delta H \quad (4.9)$$

$$h = h_{ref} + \int_{T_{ref}}^{T} C_p dT \quad (4.10)$$

T_{ref} is the reference temperature (25ºC) while h_{ref} is the value of enthalpy at 25ºC. The value of ΔH can be written in terms of the latent heat of the material, also known as the specific enthalpy of melting, L, and is calculated from the Eqn. (4.11).

$$\Delta H = \lambda L \quad (4.11)$$

The value of the liquid fraction λ is defined by Eqn. (4.12)[20][83];

$$\lambda = \begin{cases} 0, & \mathrm{T} < T_{solidus} \\ \frac{\mathrm{T} - T_{solidus}}{T_{liquidus} - T_{solidus}}, & T_{solidus} < T < T_{liquidus} \\ 1, & T > T_{liquidus} \end{cases} \quad (4.12)$$

In solidification and melting, equation $\lambda = \frac{\mathrm{T} - T_{solidus}}{T_{liquidus} - T_{solidus}}$ is referred to as the lever rule. For a complete melting-solidification cycle, PCM thermal conductivity varies according to Eqn. (4.13)[82].

$$k_{pcm} = \begin{cases} k_s\,, & \mathrm{T} < T_{solidus} \\ \frac{k_s + k_l}{2}\,, & T_{solidus} < T < T_{liquidus} \\ k_l\,, & T > T_{liquidus} \end{cases} \tag{4.13}$$

4.4 The standard *k*-ε turbulent model

For the given dimension in the modeled air duct, hydraulic diameter D_H approximates to 0.10714m. The inlet velocity of cooling air was chosen in ranges of 1 m/s, 2 m/s, and 3.0 m/s while the inlet air temperature was taken as the ambient air temperature. The resulting Reynolds numbers, Re calculated from Eq.(4.15) for the respective imposed velocities were 6860,13721, and 20582, thus all the flow regimes are turbulent. The turbulence intensity, I estimated using equation Eq.(4.14) [73], was 5.3%, 4.7%, and 4.6% for the respective Reynolds number.

$$I = 0.16Re^{-\frac{1}{8}} \tag{4.14}$$

$$Re = \frac{\rho v D_H}{\mu} \tag{4.15}$$

The turbulent flow was modelled by standard *k*-ε turbulent model. This model consists of two equations[84], one that caters for turbulent kinetic energy *k* while the other for the rate of dissipation of turbulent kinetic energy ε, respectively [85].

$$\frac{\partial}{\partial t}(\rho k) + \frac{\partial}{\partial x_i}(\rho k u_i) = \frac{\partial}{\partial x_j}\left[\left(\mu + \frac{\mu_t}{\sigma_k}\right)\frac{\partial k}{\partial x_j}\right] + P_k + P_b - \rho\epsilon - Y_M + S_k \tag{4.16}$$

$$\frac{\partial}{\partial t}(\rho \varepsilon) + \frac{\partial}{\partial x_i}(\rho \varepsilon u_i) = \frac{\partial}{\partial x_j}\left[\left(\mu + \frac{\mu_t}{\sigma_\varepsilon}\right)\frac{\partial \varepsilon}{\partial x_j}\right] + C_{1\varepsilon}\frac{\varepsilon}{K}(P_k + C_{3\varepsilon}P_b) - C_{2\varepsilon}\rho\frac{\varepsilon^2}{k} + S_\varepsilon \tag{4.17}$$

In the equations above, P_k is the production of k term, P_b caters for buoyancy and its effects on the flow, Y_M caters for the dilatation fluctuation to the overall dissipation rate,

S_k and S_ε are user-defined source terms. The constants $C_{1\varepsilon}$, $C_{2\varepsilon}$, C_μ, σ_k and σ_ε are 1.44, 1.92, 0.09, 1.0, and 1.3 while $C_{3\varepsilon}$ is calculated from Eqn. (4.18).

$$C_{3\varepsilon} = \tanh\frac{|V_b|}{|U_b|} \tag{4.18}$$

V_b and U_b , are the velocity components measured against the gravitational vector.
The value of turbulent viscosity, μ_t is evaluated from Eqn. (4.19).

$$\mu_t = \rho C_\mu \frac{k^2}{\varepsilon} \tag{4.19}$$

4.5 Thermal modeling

The performance of a photovoltaic panel is quantified on the intensity of incident radiation (W/m^2) that is converted into electrical power(W/m^2) on a given environmental condition[52]. For proper thermal modelling, the following assumptions are put into account[82].

- The temperature of the various PV module layers is spatially constant while their thermophysical properties are assumed not to vary with variations in both temperature and pressure.
- Ohmic losses in photovoltaic cells are assumed to be insignificant.
- Pressure and head losses as the fluid flows are neglected.
- The PCM is homogeneous and isotropic.
- Interfacial resistance and convection effects in the molten PCM are neglected.
- PCM density, viscosity, and thermal conductivity vary as piecewise linear with temperature.

Heat transfer through each PV layer is governed by heat transfer diffusion equation[86] expressed as in Eqn.(4.20).

$$\rho_i C_{p,i} \frac{\partial T(x,y)}{\partial t} = k_i \left(\frac{\partial^2 T_i(x,y)}{\partial x^2} + \frac{\partial^2 T_i(x,y)}{\partial y^2}\right) + q_i \tag{4.20}$$

Where $i = 1, 2 \ldots, n$ are PV module layers, q_i is the interior heat generation per unit volume of each layer.

The quantity q_i is calculated from Eqn.(4.21)[87].

$$q_i = \frac{(1-\eta_{sc})G(t)\alpha_i\tau_i A_i}{V_i} \tag{4.21}$$

η_{sc} is the electrical conversion efficiency of the solar cells. A_i and V_i are the surface area in $m^{2,}$ and volume of the solid layer of a module, respectively.

Swapnil et. al [88] discussed correlation coefficients to estimate the Evans Florschuetz cell's efficiency, therefore η_{sc} is calculated by Eq. (4.22). The equation below is the traditional linear expression for calculating the PV cell's electrical efficiency.

$$\eta_{sc} = \eta_{T_{ref}}\left[1 - \beta_{1ref}\left(T_{sc} - T_{ref}\right)\right] \tag{4.22}$$

T_{sc} is the cell's temperature, T_{ref} is considered as 25ºC at STC. The values of β_{1ref} and $\eta_{T_{ref}}$ for this study are presented in Table 4.1. The quantities $\beta_{ref}$and η_{Tref} are always provided in the PV manufacturers' specifications. The value of β_{ref}changes depending on solar cells' material[89]. The value is approximately 0.0045/K for crystalline silicon, whereas 0.0035/K, 0.0025/K, and 0.002/K are used for copper indium selenium (CIS), cadmium telluride (CdTe), and amorphous silicon solar cell, respectively. In the estimation of the reference efficiency, manufacturers use a heat flux of 1000W/m^2 as the standard test value for standard test conditions (STC) for the cells' average temperature of 25°C with 1.5m/s air velocity [90]. It is assumed that at these values, a PV generates the maximum power (Watt-peak, Wp) though in real-life operation the power generated by a PV varies with changes in both temperature and solar radiation intensity[52].

The thermal dynamic analysis on the PV module carried out by employing the energy conservation principle was applied at each layer of the PV module. The principle predicts the thermal energy of each solar component layer and determines its thermal-electrical performance [86]. The principle is expressed by the Eq. (4.23)

$$M_i C_i \frac{dT_i}{dt} = \sum_{in} Q_i - \sum_{out} Q_i \tag{4.23}$$

where,

$M_i C_i \frac{dT_i}{dt}$ is the stored or generated energy in or by component i of the PV module. $\sum_{in} Q_i$ and $\sum_{out} Q_i$ are the total energy received or lost by component i when the radiation falls in the panel, respectively.

The modified energy equations were applied to the PV cell to estimate total, thermal and electrical energy. Modifications of the energy balance equations for the PV module were done by Cox and Raghuraman[91]. The total energy, E_C absorbed by the PV cell neglecting effects of interreflection of solar irradiation between various surfaces of the module and thermal absorption by the glass cover, was evaluated by Eq. (4.24), where $\alpha_{sc}$is solar cell's absorptivity.

$$E_C = \beta_{sc}\alpha_{sc}\tau_g G(t) \tag{4.24}$$

As solar irradiation reaches the surface of the module, a fraction of it is transformed into electrical energy. The magnitude of electrical energy, E_{CE} produced by a PV cell is evaluated by Eq. (4.25).

$$E_{CE} = \beta_{sc}\eta_{sc}\tau_g G(t) \tag{4.25}$$

A fraction of the incident radiation that is dissipated as heat constitute the thermal energy, E_{CT} which is evaluated by Eq. (4.26).

$$E_{CT} = (1 - \frac{\eta_{sc}}{\alpha_{sc}})\beta_{sc}\alpha_{sc}\tau_g G(t) \tag{4.26}$$

The rate at which the back sheet material absorbs solar energy after successive transmission through the module layers is given by Eq. (4.27), where $\alpha_T$is the absorptivity of the material.

$$E_T = \tau_g(1 - \beta_{sc})\alpha_T G(t) \tag{4.27}$$

The principle of energy conservation can now be expounded on each component of the PV module as shown below:

$$\left(1 - \frac{\eta_{sc}}{\alpha_{sc}}\right)\beta_{sc}\alpha_{sc}\tau_g G(t) + \tau_g(1 - \beta_{sc})\alpha_T G(t) = q_c + E_{loss} \tag{4.28}$$

Where E_{loss}, is the total energy lost to the environment from the top glass layer. Losses are either convection (free and forced) or radiation. Free convection occurs near the surface of

the glass layer as a natural buoyance force as the temperature of air increases. Forced convection is a result of wind.

$$E_{loss} = h_g\left(T_g - T_{amb}\right) + \varepsilon_g \sigma {T_g}^4 - \alpha_g \sigma (T_{amb} - 6)^4 \quad (4.29)$$

h_g is the forced convection heat transfer coefficient of the glass layer[92]. T_g, T_{amb} and ε_g are the temperature of the glass layer, the ambient temperature, and emissivity of glass while the quantity $(T_{amb} - 6)$°C is sky temperature[92], and σ is the Stefan–Boltzmann constant ($W/m^2\ k^4$).

$$h_g = 1.247(\left[T_g - T_{amb}\right] \cos\theta)^{\frac{1}{3}} + 2.658V_w \quad (4.30)$$

Where, θ, is the angle of tilt of the PV module. Angle, $\theta = 0°\text{C}$ for the current study.

The value of q_c, is estimated by Newton's law of cooling and calculated from Eq. (4.31).

$$q_c = h_B(T_b - T_{amb}) \quad (4.31)$$

$$h_B = 2.8 + 3V_w \text{[93]} \quad (4.32)$$

Where, T_b is the temperature of the back sheet material and V_w is the wind velocity.

4.6 Modelling and analysis of EAHE.

The design specifications and dimensions are decided according to the data from the selected sites and the heating loads of the system. The designer identifies the input parameters and those that affect the heat transfer process. Once that done, heat transport equations are taken into considerations with assumptions such that the desired output is met. The input parameters include the inlet air mass flow rate ṁ, temperature T_{in} while the output parameter is only the air temperature from the outlet of EAHE, T_{out}. The main factors that affect performance of EAHE include the thermal conductivities of both soil and pipe, the diameter, length, thickness, number of pipes and the EUT[76], [94]. These are parameters considered when the sizing problem.

To simplify the modelling of a one-dimensional EAHE system, the following assumptions are put into considerations.

- The earth's surface temperature and the inlet air temperature are assumed to be equal to the ambient air temperature.
- The earth's undisturbed temperature, EUT is approximated as the annual average temperature of the location.
- The cross-section area of air ducts (polyvinyl chloride, PVC) is assumed uniform throughout the system.
- A small pipe thickness is assumed thus a negligible thermal resistance of pipe material.
- The pipe surface temperature is assumed to be axis symmetrical and uniform.

In this study, heat transfer rate is estimated by the ε–number of transfer units (ε–NTU) method. In the EAHE, air is the only medium used for heat transportation.

Since the expression of NTU is dependent on flow configuration used in a heat exchanger system, the similarity of evaporator or condenser having a non-varying temperature on one side is used for estimation of NTU.

The total heat energy transferred from the air as it flows in the buried pipes is given by Eqn. (4.33).

$$Q_h = \dot{m} C_p (T_{out} - T_{in}) \tag{4.33}$$

where

$$\dot{m} = \frac{\frac{\pi}{4} D^2 \rho_a v_a}{N_p} \tag{4.34}$$

Convective heat transfer between the wall of the pipe and air is given by Eq. (4.35).

$$Q_h = hA\Delta T_{lm} \tag{4.35}$$

In the expression above, h is the convective heat transfer coefficient (W/m^{2}K), A is pipe inner surface area (m^2), and ΔT_{Im} is the logarithmic average temperature difference.

$$\Delta T_{Im} = \frac{T_{in} - T_{out}}{\ln\left\{\frac{T_{in} - T_{wall}}{T_{out} - T_{wall}}\right\}} \tag{4.36}$$

Where $T_{wall} =$ EUT

The air temperature at the outlet of the EAHE is obtained in exponential form by the elimination of Q_h from Eqn. (4.33) and (4.35).

$$T_{out} = T_{wall} + (T_{in} - T_{wall}) e^{-(hA/\dot{m}C_p)} \tag{4.37}$$

When an infinitely long pipe (A = ∞) is used, cooling or heating is accounted by the wall temperature and thus the effectiveness (ε) of the system is defined as:

$$\varepsilon = \frac{T_{out} - T_{wall}}{T_{in} - T_{wall}} = 1 - e^{-(hA/\dot{m}C_p)} \tag{4.38}$$

The dimensionless expression NTU is expressed by Eq. (4.39).

$$\text{NUT} = \frac{hA}{\dot{m}C_p} \tag{4.39}$$

4.6.1 Design parameters.

The design parameters considered for the EAHE system are scaled to enable modelling as follows. A PVC pipe of diameter 1 inch, with a buried length of 5m was used. The horizontal arrangement of the EAHE was adopted with the pipes spaced by 200mm. The radius of curvature of the pipe was 200mm. The PVC pipe was buried 3m below the ground surface**.**

4.7 Boundary conditions

The PV module is exposed to solar radiation, $\boldsymbol{G(t)}$ of $\mathbf{540}$ W/m^2, the average hourly direct solar irradiation in Uganda [79], and an air film coefficient of 8 W/m^2 K with an

ambient air temperature of 26ºC. A portion of the incident radiation is reflected $\boldsymbol{q_r}$. $\boldsymbol{q_{conv}}$ accounts for convection and radiation losses on the PV module surface. Ethylene Propylene Diene Monomer (EPDM) of thickness δ mm is used to provide insulation[71] for the PCM domain (Fig.4.2). At PCM-metal interfaces conservation of energy is satisfied.

$$\boldsymbol{k_{alm}\frac{\partial T}{\partial y} = k_{pcm}\frac{\partial T}{\partial y}} \tag{4.40}$$

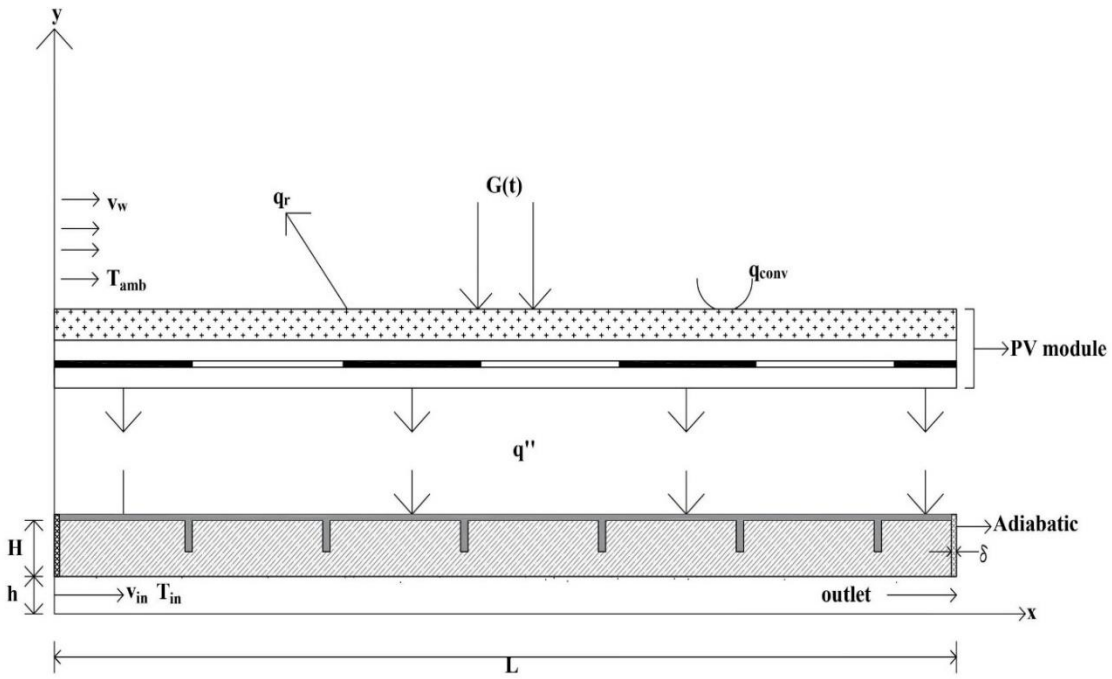

Figure 4.2: Schematic cross-section of configurations with boundary conditions.

At $y = (H + h)mm$ heat flux from the module is received by the copper domain as

$$q'' = -k_{copper}\frac{\partial T}{\partial y}\Big|_{\mathrm{y=H+h}} \tag{4.41}$$

At the air inlet of the cooling channel, shown in Fig 4.2, $(x = 0, 0 \le y \le h)$

$$u(0,y) = U_{in}\,, \quad v(0,y) = 0, \;\; T(0,y) = T_{in}$$

A pressure outlet is assigned at the air outlet, $(x = L, 0 \le y \le h)$ where the gauge pressure is zero (0)

No-slip boundary conditions were imposed on the air-metal interface in the air duct.

At $(y = 0, 0 \le x \le l)$, the boundary condition is:

$$k_{air}\left.\frac{\partial T}{\partial y}\right|_{x,0} = h_B(T_{amb} - T_{(x,0)}) \quad (4.42)$$

where, T_{amb} is the ambient air temperature and h_B is the heat transfer coefficient from the rear end to the surrounding in W/m^{2}K.

At the inlet of the Earth-to-air heat exchanger, the velocity of the air was taken as 3m/s, and the static temperature of the air, T_{in} was taken as 41°C, a value corresponding to the maximum ambient air temperature of India under the studied conditions. The flow was taken as turbulent corresponding to Reynold's number of 4761 and turbulent intensity, I of 5.55%. The thermal properties of the EAHE materials used in the model are presented by T. S. Bisoniya [95]. A pressure outlet was assigned with the relative air pressure is 0. The external pipe wall temperature was taken as axis symmetrical and uniform and equal to EUT of central India i.e., 25.2 °C[95] while at the inner surface, no-slip conditions were assigned.

4.8 Validation of results

The numerical simulation of the PVT module was validated by comparison again experimental results conducted by M. Sardarabadi et al using weather data for Ferdowsi University of Mashhad, Mashhad, Iran [96]. Due to long computation time, only data for 7 data points are illustrated in Fig.4.3. The total difference between numerical results of current study and experimental results presented by M. Sardarabadi et al was found to be 3.1°C. It should be noted that the discrepancy in result may be due to assumptions during modelling and experimental errors.

The PCM domain is validated using experimental results from Kamkari et al.2014[97]. Kamkari et al investigated the effect of inclination angle on convection-driven melting of a lauric acid PCM enclosed in a rectangular container. A 50mm by 120mm-by-120mm inner dimensional container was used in the study.

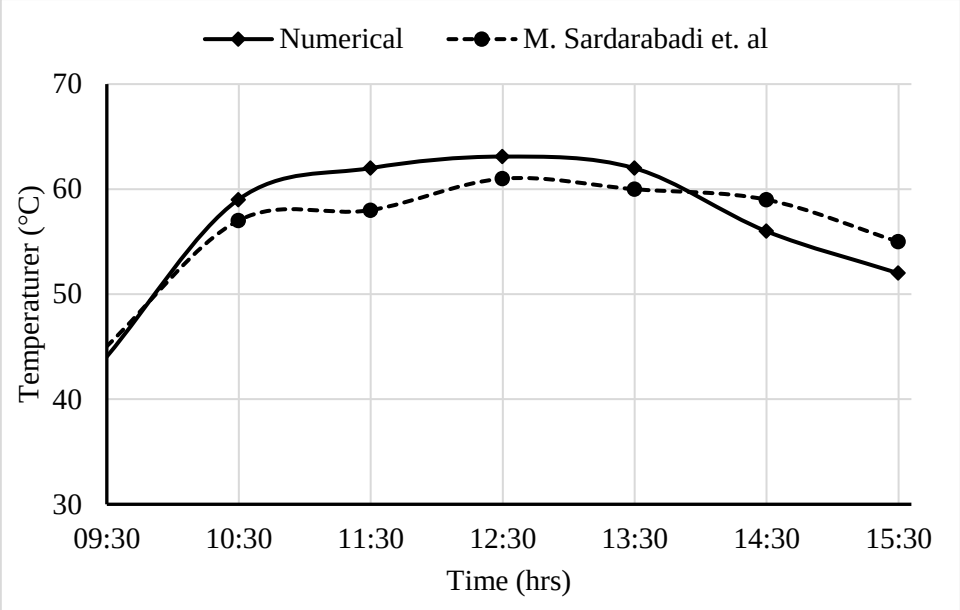

Figure 4.3:Experimental and numerical results for PV-module.

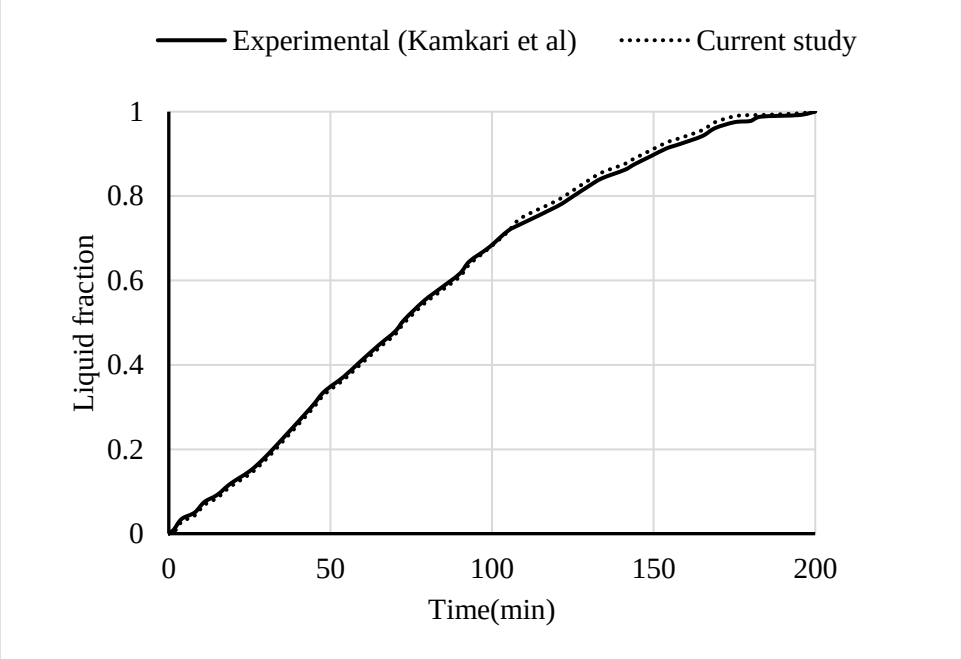

Figure 4.4:Variation of the liquid fraction of lauric acid PCM with time.

A constant temperature heat exchanger was used to keep the right side of the PCM encloser at a temperature of 70°C. The other walls were made of a 25 mm thick transparent plexiglass sheet of low thermal conductivity for easy visualization and to minimize heat

losses. Further insulation was realized by the addition of 3cm thick ethylene propylene diene monomer (EPDM) sheets. Sets of T-type thermocouples were employed for result realization. The resulting plot of melt fraction against flow time was compared with the current study simulation under the same conditions and parameters. The graphs as shown in Fig.4.4 exhibited a better agreement.

CHAPTER

RESULTS AND DISCUSSION

5.1 Solar flux distribution

In this work, a novel approach for incident solar radiation modelling based on solar ray tracing (path-tracing) is presented. The solar radiation was treated perpendicularly incident on the solar module. The reflected, transmitted, and absorbed solar fluxes are presented in Table 5.1.

Table 5.1: Solar radiation distribution.

	Visible solar flux (W/m^2)	Infrared solar flux (W/m^2)
Absorbed	163.458	163.458
Reflected	52.542	52.542
Transmitted	54	54

Only 20% of the incident $540W/m^2$ was transmitted, 19.56% reflected while 60.54% was absorbed. Most of the radiation occurs between visible a light region of 400nm to 700nm for an air mass of Zero (0). For this reason, solar cells must absorb as much energy as possible in the visible region of the solar radiation spectrum[13]. The biggest fraction of the absorbed infrared radiation attributes to the heat on the solar module[98]. The module produces $326.916W/m^2$ of solar heat flux.

5.2 PV Module Surface temperature

A conventional photovoltaic system was modelled for comparison purposes to investigate the effect of the recommended cooling mechanism on the PV cells. The analytical solution to this model includes energy balance of all PV layers exposed to solar irradiation.

Numerically, the maximum temperature of the solar cell surface was found to be 60.1ºC for a conventional PV Module. Temperature contours for the studied module configurations are presented in Fig 5.1.

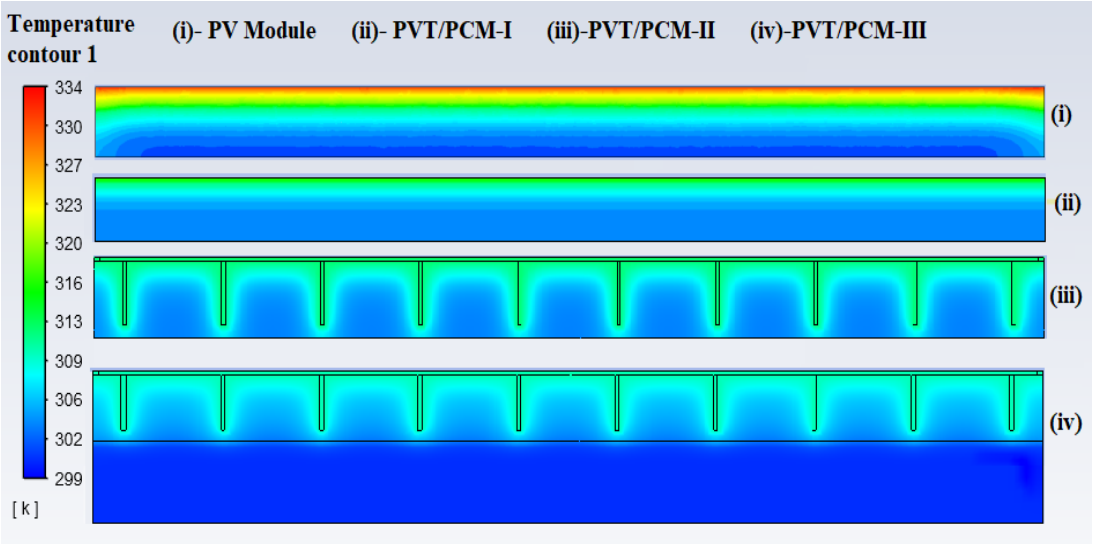

Figure 5.1: Temperature contours for module configurations (After 120 minutes).

When a pack of RT35 PCM was added to the PV panel, surface temperature was reduced by approximately 33.4% as illustrated in Fig. 5.2. When the incident solar radiation strikes the surface of the PV, its temperature raises. Eventually, the surface of PCM in contact with the rare end of the PV module receives the heat energy and at a particular point, the PCM starts melting absorbing thermal energy from the module[19]. The heat energy that would raise the PV temperature is used in a phase transition. Melting continues so long as the PV module is exposed to solar radiation. As the temperature of the module falls below the melting point, the PCM starts solidifying releasing thermal energy to the ambient. This phase transition provides a useful effect on the overall efficiency of the PV module. The introduction of high conductivity copper fins in the PCM, as in PVT/PCM-II increases the surface area over which heat transfers. This increases the heat transfer rate inside the PCM[70], thus enhancing their thermal energy absorption capacity. Fins also act as pressure release passage for molten PCM[99]. In this study, a 5% reduction in surface temperature was registered by embedded fins in the PCM domain. Furthermore, a 5mm increase in the fin height resulted in a minimal drop of about 0.7% in the surface temperature. The maximum

number of fins was chosen as 10 even though an increased number of fins would aid in reducing the thermal stratification. Increasing the number of fins may on the other hand result in system failure due to increased system weight.

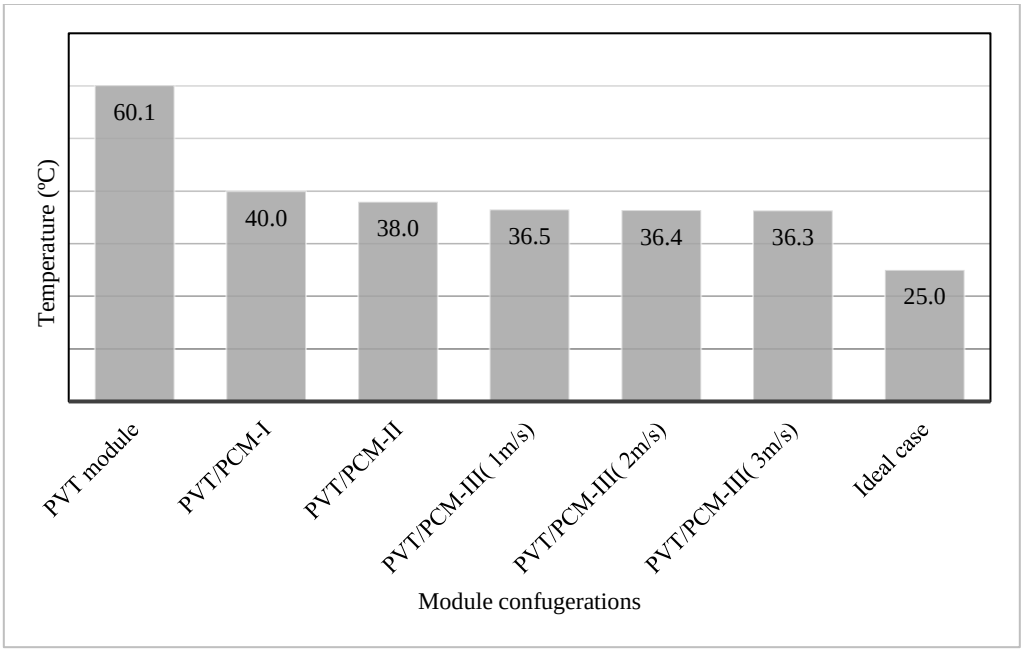

Figure 5.2:Surface temperature for the respective configurations.

For PVT/PCM-II, a further increase in the magnitude of solar irradiation or a raise in ambient air temperature may at a particular point change the liquid fraction of the PCM to entirely l, as shown in Fig. 5.8, thus no further thermal energy will be absorbed. This occurs when the PCM has reached its peak equilibrium temperature upon complete phase transition. At this point, the PCM acts as a heat source, contributing to the rise in cell surface temperature. It was, therefore, important to cool the rear surface of the PCM with a cooling fluid as in PVT/PCM-III. The cooling effects play two roles: keeping the value of the liquid fraction less than 1, thus retarding complete phase transition and contributing to a further reduction of PV surface temperature by 4.5%. A unit increment in the inlet air velocity stemmed in a 0.27% reduction in PV cell surface temperature.

5.3 Fin number optimization.

The variation of solar cell surface temperature for different numbers of fins in the PCM domain is illustrated in Fig.5.3. As expected, a reduction in surface temperature was observed with an increase in fin number. Temperature reduction is due to the increased heat transfer surface area resulting from increased fin number. After 15 fins, however, the rate of temperature reduction was minimal. Further addition of fins would increase the overall system weight and hence the cost. Therefore, the optimal range of fin numbers for an observable temperature reduction is 10-15 fins. The maximum number of fins was chosen as 10 for this study.

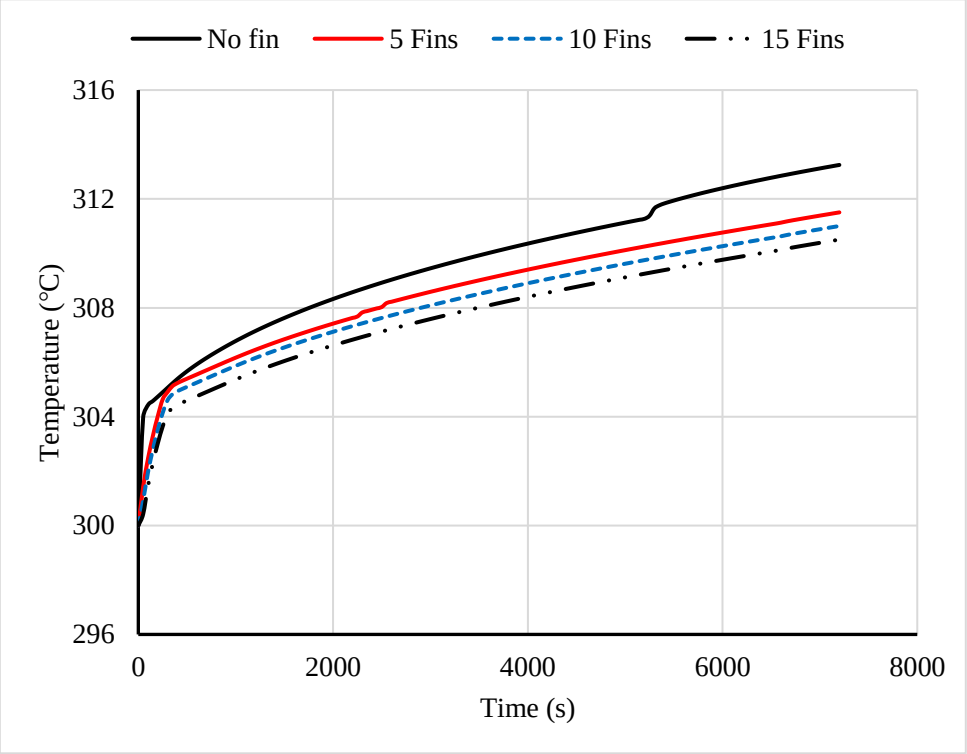

Figure 5.3: Solar cell surface temperature variation with fin number.

The amount of solid-state PCM need per hour for thermal management is estimated from the relationship between heat energy and the latent heat, λ of RT35. The studied PVT module (Fig. 5.1(i)) produces an estimated solar heat flux of 326W/m^2 for an area of 0.25m^2. This corresponds to 81.729W heat energy Q to be removed from the PV module by the

suggested cooling method. Heat energy to be removed is equal to the latent heat, λ of RT35 on an hourly basis[19]. Thus,

$$Q = m\text{x}\lambda, \text{ where } m \text{ is the mass(kg) of the PCM.}$$

$$81.729\text{x}3600 = m\text{x}160000$$

$$m = 1.84kg\ per\ hour.$$

The volume of the PCM, $v = mass(m)/\ RT35\ solid\ state\ density.$

$$v = 1.84/860 = 2.14x10^{-3}m^3\ \ per\ hour.$$

5.4 Effect of solar cell surface temperature on power production.

The energy balance equations, Eqn. 4.24-4.26 for the Photovoltaic module modified by Cox and Raghuraman [5] [91] were applied to estimate the total absorbed energy, electrical energy, and thermal energy. At standard test conditions (STC) [52], a performance of 20% can be expressed as electrical energy production of 200W/m^2. For the studied module under the studied climatic data, specific electric power produced is 75.3 W/m^2,83.39 W/m^2, 84.19 W/m^{2,} and 89.42W/m^2 for the respective module configurations. The specific thermal power produced for the respective configuration as a function of surface temperature includes 327.11 W/m^2, 319.02 W/m^2, 317.53 W/m^{2,} and 312.98 W/m^2. Thermal power reduction of about 2.5%, 3.0%, and 4.3% was registered by opting PVT/PCM-I, PVT/PCM-II, and PVT/PCM-III respectively over PVT Module configuration.

5.5 Effect of cell surface temperature on electrical efficiency.

Solar cell electricity conversion efficiency was calculated using Evans Florschuetz PV efficiency equation Eq. (4.22) [88]. For the time-dependent cases, the variation of solar cells' electrical conversion efficiency with time is presented in Fig.5.5. Conversion efficiency varies inversely with time. it was found out that the efficiency in PVT/PCM-III is always greater than that for PVT/PCM-II and PVT/PCM-I. For the respective module

configurations, the efficiency reached 16.84%, 18.56%, 18.83%, and 18.98% as shown in Fig.5.4. A percentage increase in efficiency of 10.75%,11.82%, and 12.71% was registered by using PVT/PCM-I, PVT/PCM-II, and PVT/PCM-III respectively over PVT module configuration.

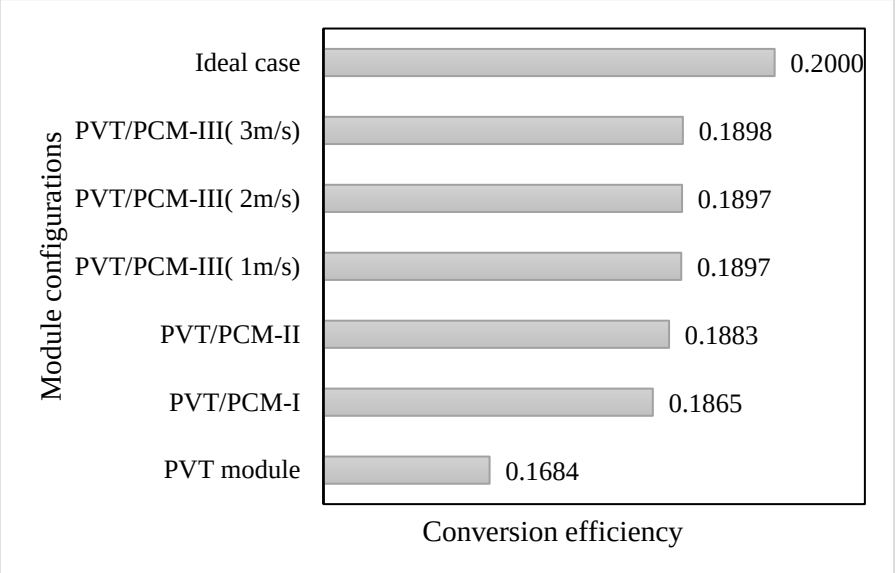

Figure 5.4:Electric conversion efficiencies for PV configurations.

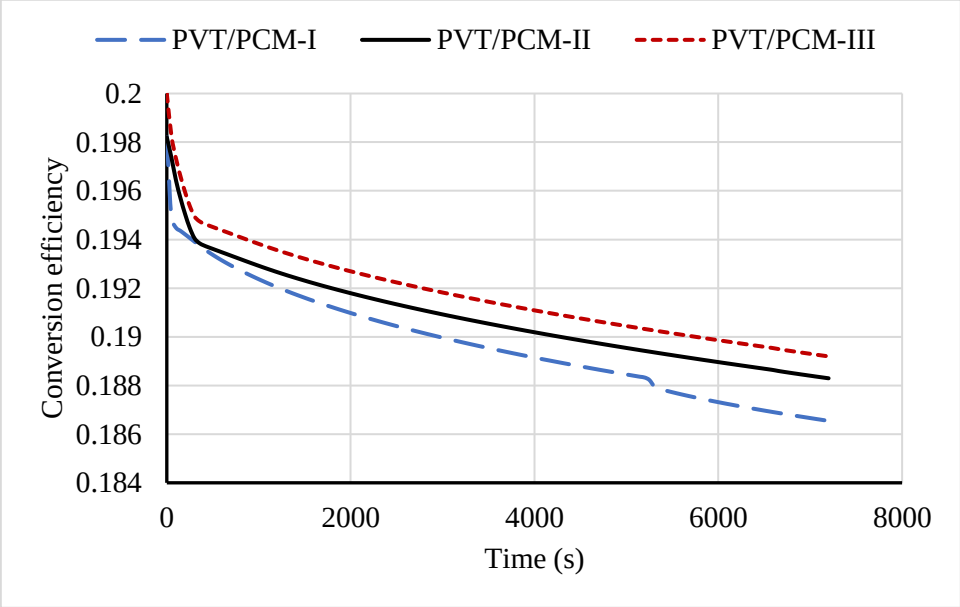

Figure 5.5: Solar cell electrical conversion efficiency against computation time.

5.6 Effect of module configurations on temperature profile.

A plot of cell temperature against computation time, observing the rate of increase of cell temperature is shown in Fig.5.6. The temperature of the PV Cells increases steeply to about 303K for the first 200 seconds for PVT/PCM-I. Within this range, the PCM is still solid. At 303k, the heat energy that would raise the cells' temperature is absorbed by the melting PCM. This lowers the rate at which surfaces temperature increases for the remaining 7000 seconds. The rate at which temperature rises in PVT/PCM-II is higher than that in PVT/PCM-III for the entire 7200 seconds of the simulation time. The additional cooling effect at the rear end of the PCM provided by the air accounts for this reduced rate of temperature increase in PVT/PCM-III.

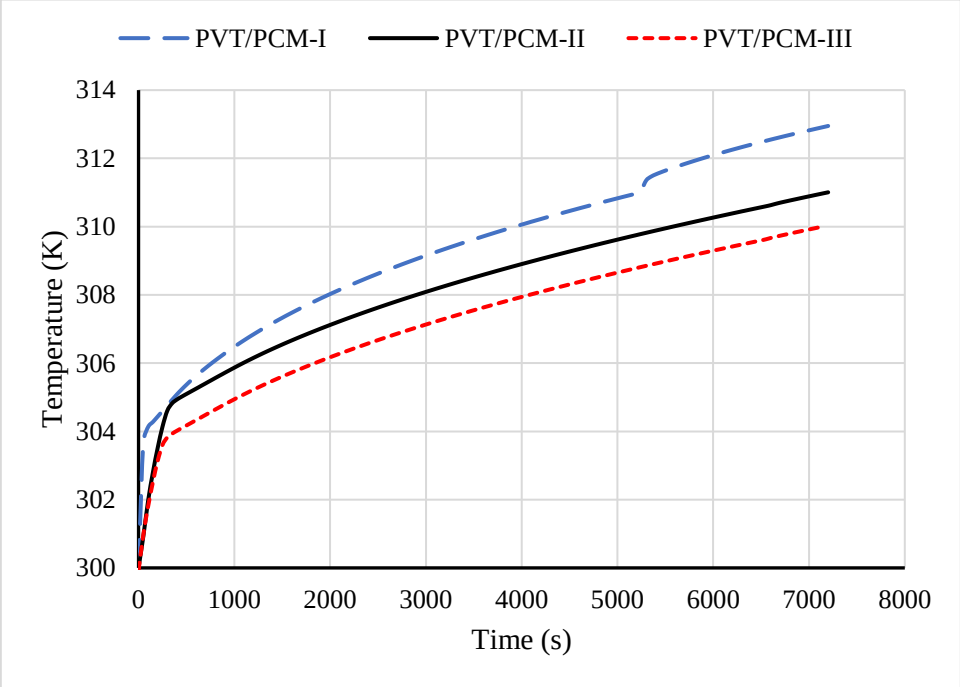

Figure 5.6: Comparison of the solar cell temperature profile.

5.7 Effect of inlet coolant air temperature on solar cell temperature

A reduction in the air temperature at the inlet in PVT/PCM-III reduces the PCM rate of melting thus enhancing its thermal absorption capacity. According to Fig.5.7, we can conclude that a 1% reduction in coolant air temperature results in a near 3°C reduction in the cell temperature.

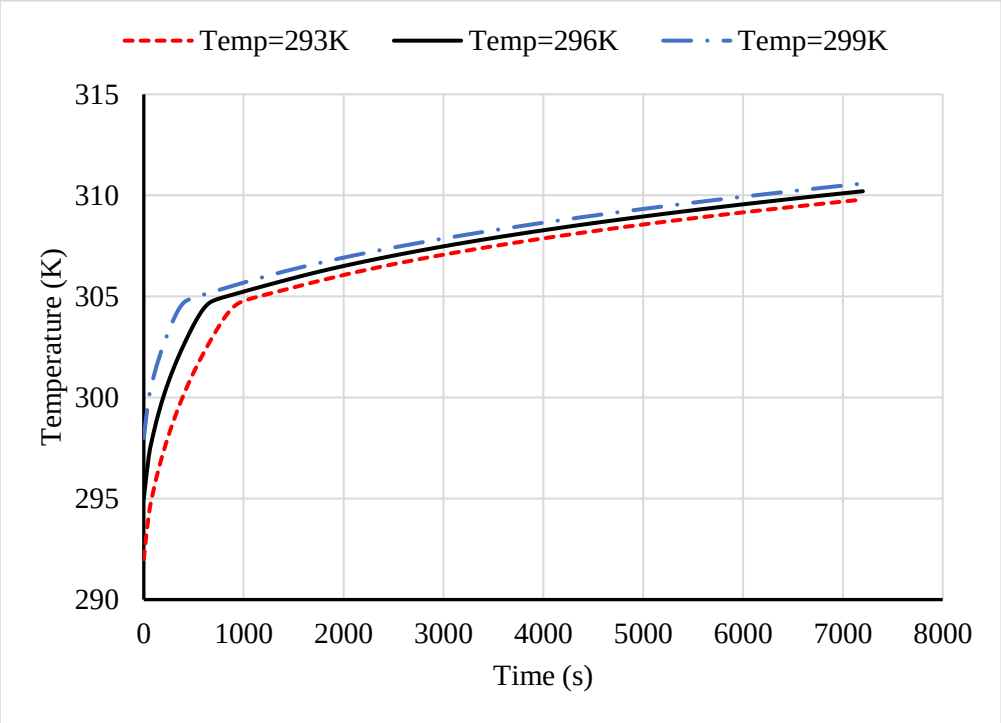

Figure 5.7: Influence of inlet air temperature on the PV cell surface temperature.

5.8 Effect of module configuration on the melting rate of PCM

Figure 5.8 compares the melt fractions of RT35 for different module configurations within the first 2 hours of exposure to solar radiation. For PVT/PCM-I, the PCM starts melting after the first 100 seconds. Between the interval of 0 to 100 seconds, the PCM is entirely solid as heat energy is absorbed by the PV module layers. For PVT/PCM-II and PVT/PCM-III, melting commences after 200 seconds and gradually increases up to a complete phase change. A complete phase transition occurs after 5250 seconds, 6600

seconds, and 6950 seconds for PVT/PCM-I, PVT/PCM-II, and PVT/PCM-III, respectively. Thus, the melting rate is higher in PVT/PCM-I than in all other configurations. This means that PVT/PCM-III absorbs and stores more thermal energy than all other configurations.

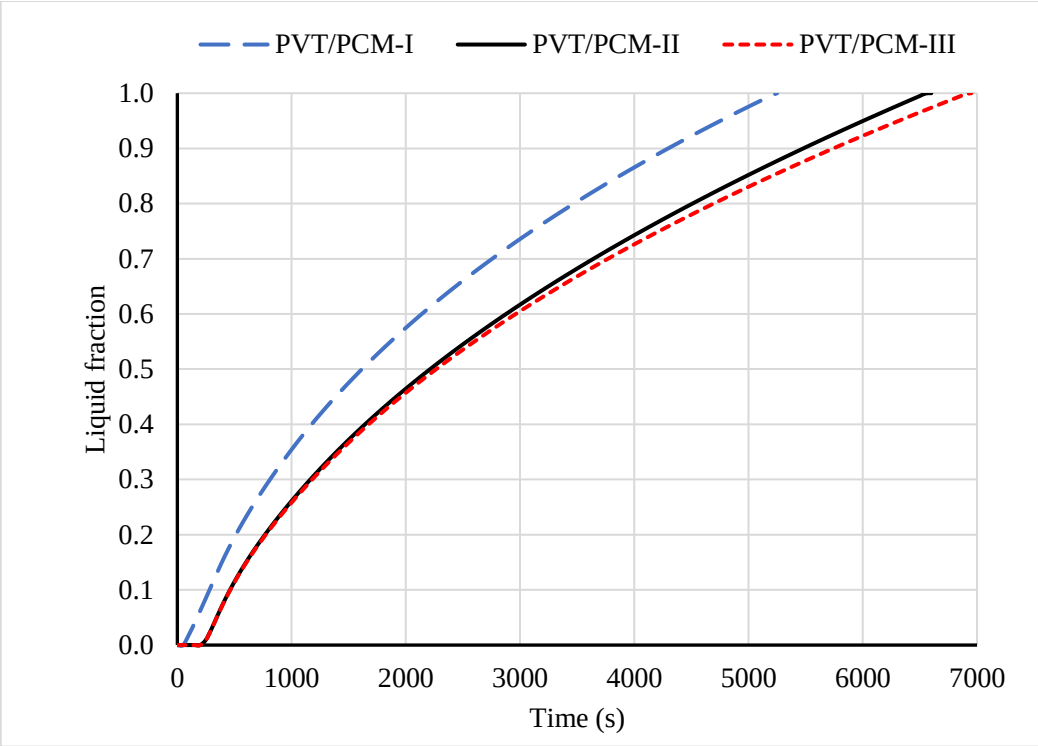

Figure 5.8: Comparison of PCM melt fraction for various Module configurations.

5.9 Effect of PCM melting temperature on cell temperature.

The thermal response of PVT/PCM-III with changes in PCM melting temperature was evaluated under the studied conditions with inlet air flowing at 3m/s. The rest of the thermophysical properties of the PCM were kept unaltered. A study was conducted for PCM melting temperatures of 29°C, 34°C, and 54°C. For the two hours of simulation time, the results indicate that an increase in PCM melting temperature results in an increased cell temperature because of the decreased melting rate. Cell temperatures of 36.3°C, 39.4°C, and 44.1°C were registered for the respective melting temperature. Thus, to maximize efficiency, a PCM with a low melting temperature should be used.

5.10 System verification.

After the comparative study, the most efficient configuration, PVT/PCM-III, was verified against weather data of two selected locations in India[100], and Algeria[101]. The main aim for this was to verify the model's efficiency and power output under real environmental conditions.

5.10.1 Renewable Energy Development Centre, Bouzaréah, Algeria.

Data presented by Slimani et al[101] in Fig.5.9 indicate ambient air temperature on 12th June 2013 was less than the melting temperature of the PCM used in this study throughout that day. Thus, PVT/PCM-III was employed without any further modifications. Latitude 36.8N, longitude 3.12E, azimuth 20°, and altitude 345 m are geographical coordinates of the site location consider for verification. Ten data points were simulated assigning a mixed boundary condition on the PV module surface to cater for the effect of natural convection and external radiating panel temperature. PVT module and PVT/PCM-III were simulated to cater for a conventional PV and a cooled PV module, respectively. Graphs of PV cell surface temperature and conversion efficiency are illustrated in Fig 5.10.

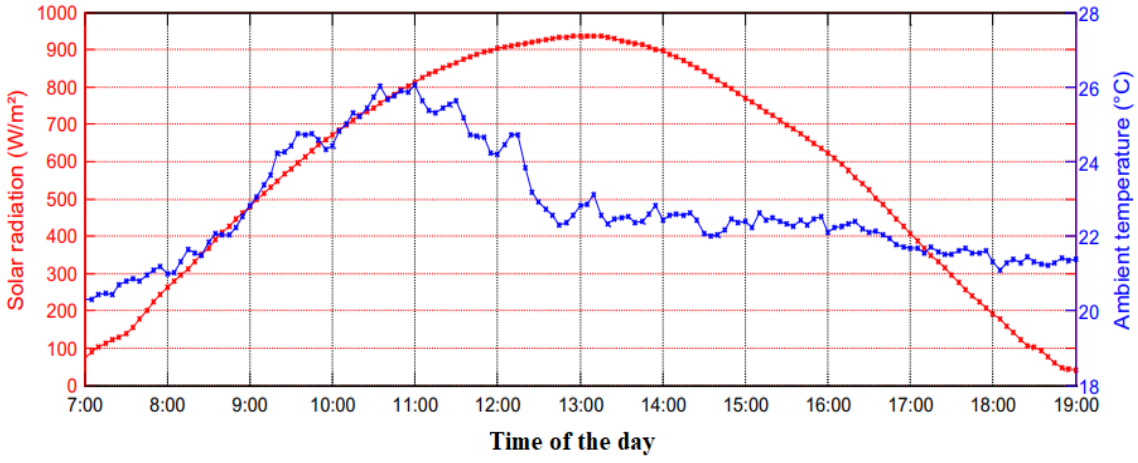

Figure 5.9: Daily temperature and irradiation for Bouzaréah, Algiers, Algeria[101].

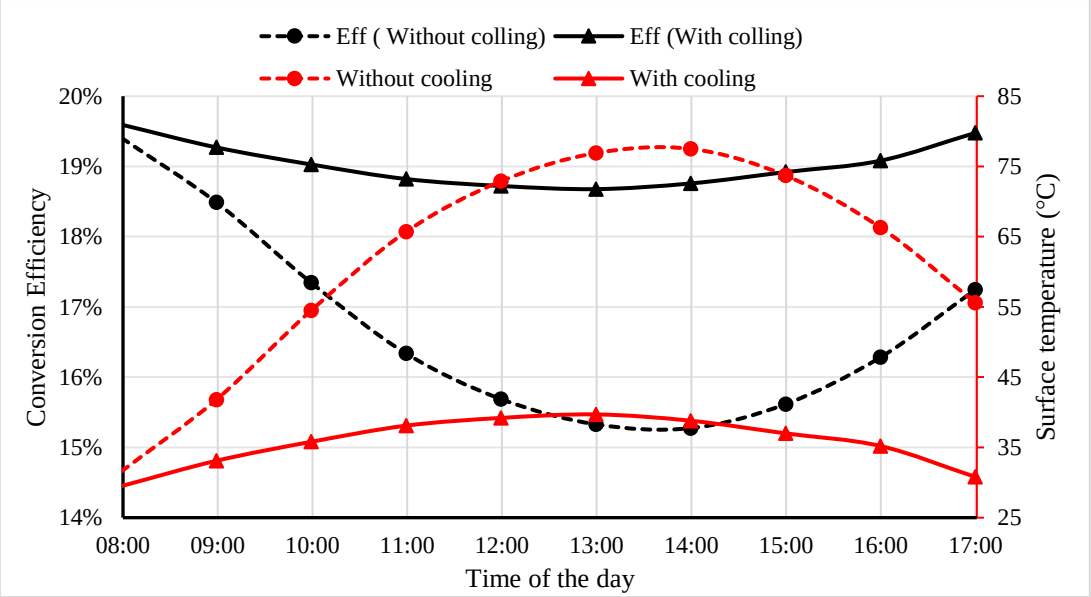

Figure 5.10: Efficiency and surface temperature against time for a site in Algeria.

The use of PVT/PCM-III lowers the surface temperature to more than half the value when a convention PV module is used between 11:00 Am to 3:00 Pm. During morning hours, when the radiation is low, the cooling effect of PCM is minimal. The hourly variations of electrical conversion efficiencies for a PV module with and without cooling effect were calculated. Efficiency range between minimum values of 15.3% and 18.7% and maximum values of 19.4%and 19.6% for a conventional PV and PVT/PCM-III at 1:00 Pm and 8:00 Am, respectively.

5.10.2 Solar Energy Park, Indian Institute of Technology-Delhi, India.

Data presented by Joshi et al [100] in Fig.5.11 showed that hourly ambient air temperature for a particular day of May 2007 was always higher than the melting temperature of the PCM selected for the study.

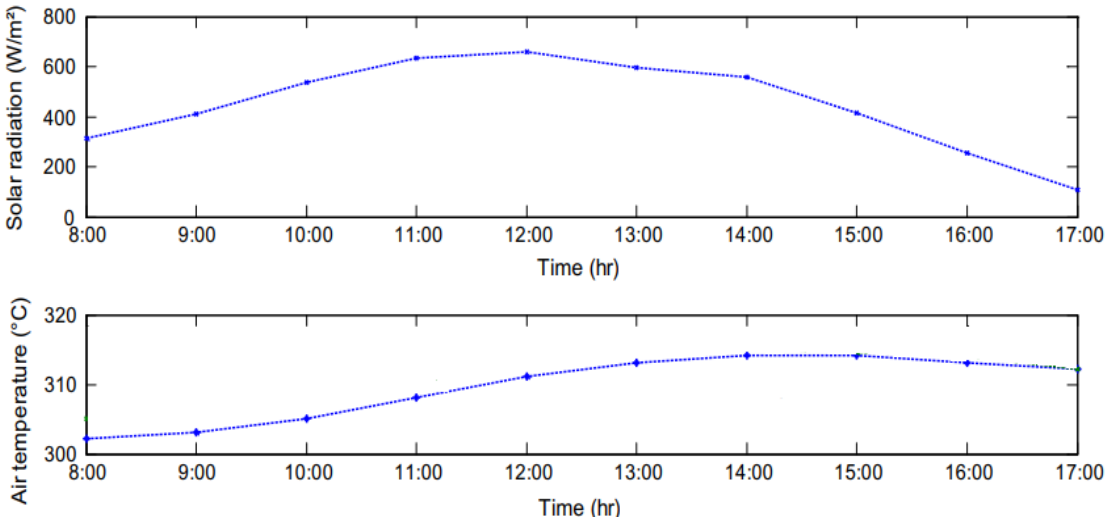

Figure 5.11: Daily temperature and irradiation for Solar Energy Park[100]

This limits the direct adoption of the PVT/PCM-III. Various modifications were to be done to directly apply PVT/PCM-III for analysis under these conditions. To adopt the studied model, the inlet coolant air was further cooled using an earth-to-air heat exchanger. The EAHE model was developed using earth's undisturbed temperature (EUT) of central India provided by Bisoniya, 2015 [95].

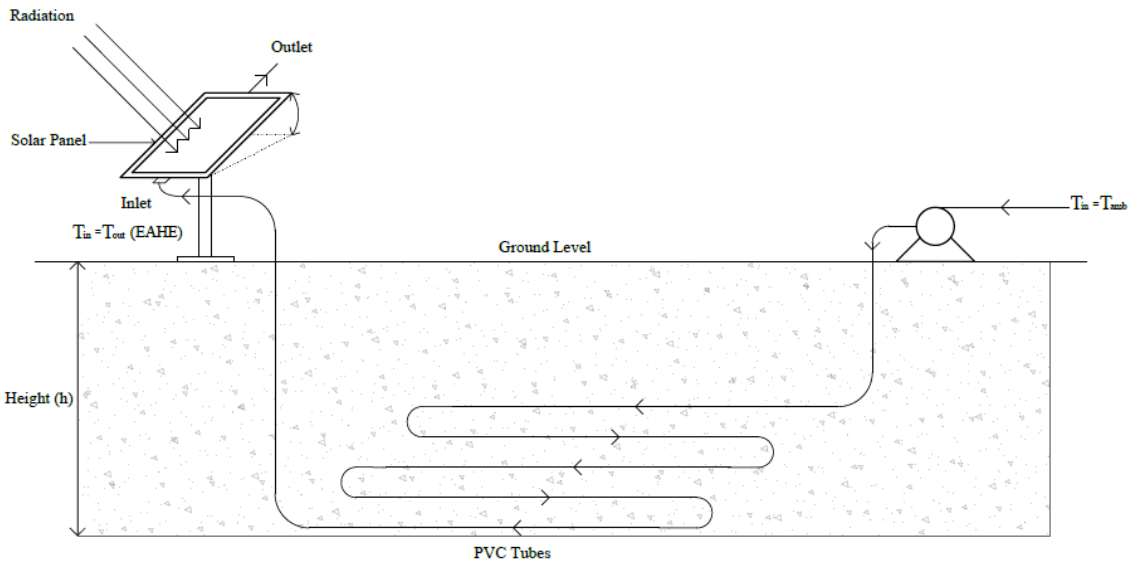

Figure 5.12: schematic diagram of PV -EAHE system.

At the inlet, air at a velocity of 3m/s, and the static temperature T_{in} of 41°C, a value corresponding to the maximum ambient air temperature of India under the studied conditions was blown in by an external device such as a blower. Air from a pressure outlet of the EAHE was ejected into the inlet of the cooling duct underneath the PCM layer of PVT/PCM-III. The EAHE system was subjected to the given boundary conditions. It was found out that the coolant air temperature would be reduced to 25.84°C throughout the day when a longer polyvinyl chloride pipe of 5m was used and buried at 2 feet below the ground as presented in Fig 5.12 and Fig 5.13.

The addition of an earth-to-air heat exchanger enables solar cell surface temperature to be cooled below the ambient air temperature. This is because the rate at which heat is absorbed by the solar cells from the sun is kept lower than the rate at which the PCM absorbs heat from the solar panel.

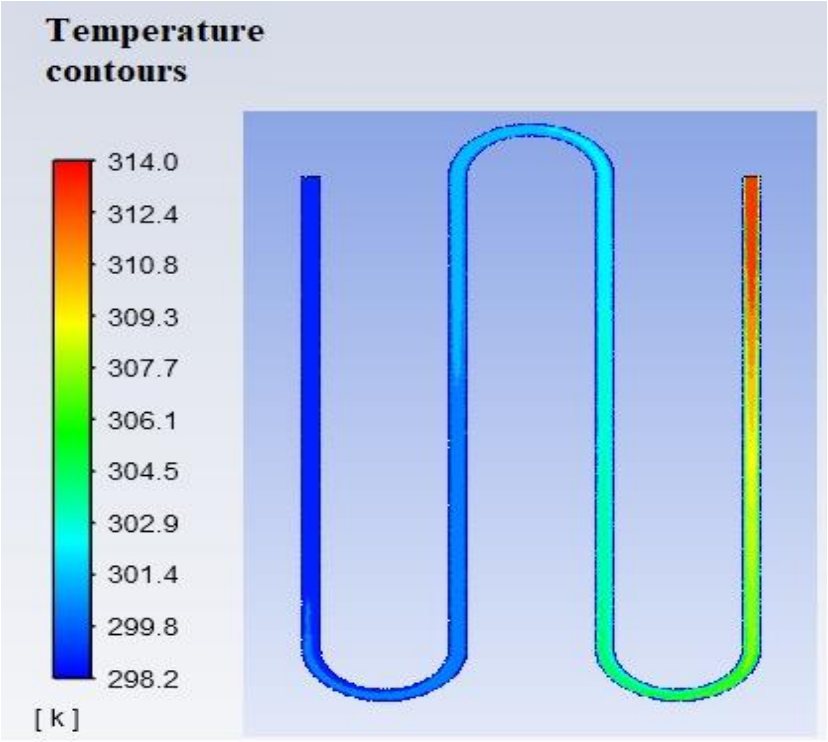

Figure 5.13:Temperature contours for EAHE: At the inlet (a), At the outlet (b) after one hour.

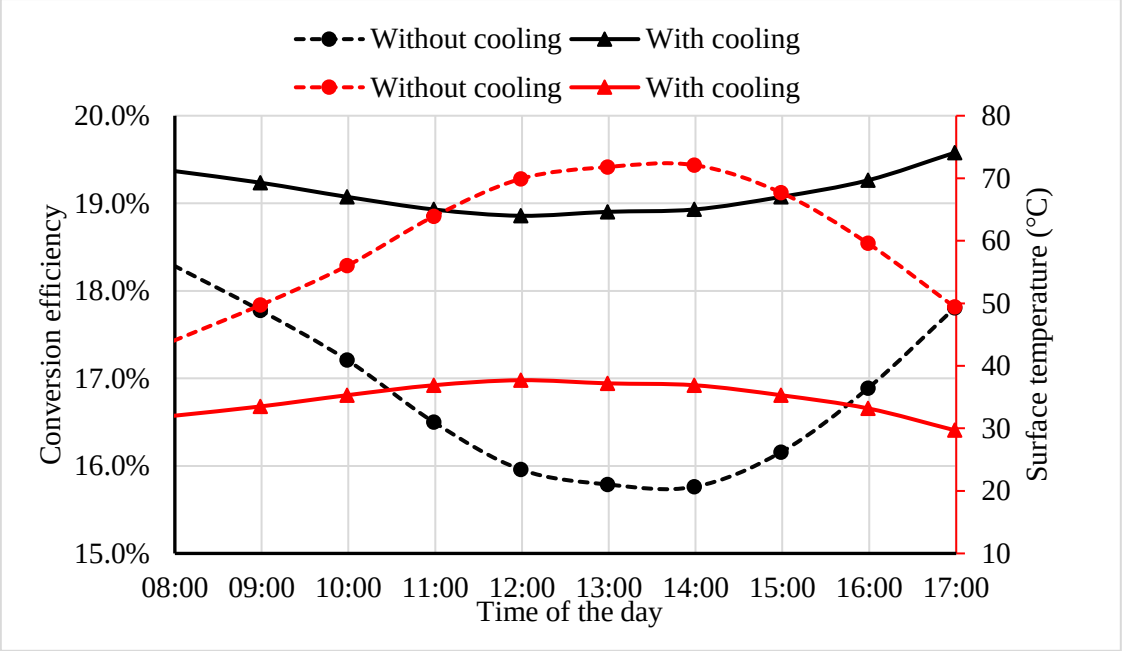

Figure 5.14: Efficiency and surface temperature against time for a site in India.

It is evident in Fig.5.14 that at noon, the solar cell was cooled to 32.01°C registering the lowest efficiency of 18.86% while at 5:00 Pm the highest efficiency of 19.58% was registered with 29.7 °C surface temperature. This indicates that solar cells' efficiency mainly depends on how effectively their surface is cooled but not the magnitude of solar radiation.

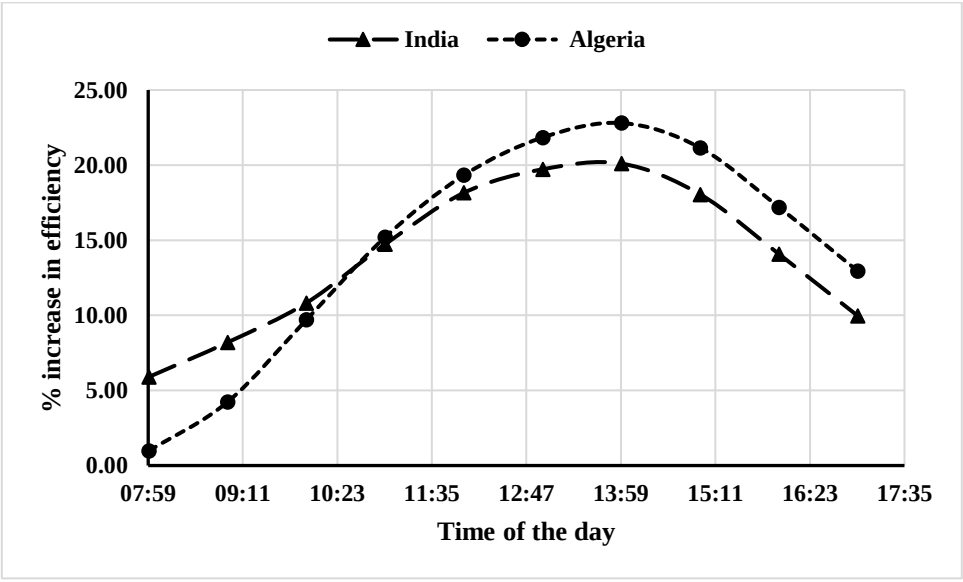

Figure 5.15: Hourly percentage increase in efficiency for the selected places.

Figure 5.15 compares the rate of increase of conversion efficiency overtime during the day for the two locations. Between 8:00 Am to around 10:30 Am, increase in efficiency is generally linear though the magnitude of the increase is more in India than in Algeria. Between 11:30 Am to 5:00 Pm efficiency increased more in Algeria than in India. The rate of increase in efficiency represents the importance of cooling the solar systems.

5.10.3 Comparison in power produced.

The variations of electrical and thermal power produced per unit area of solar cell with local time while the conventional PV is used and when PVT/PCM-III in for the selected locations are compared in Figures.5.16 and 5.17.

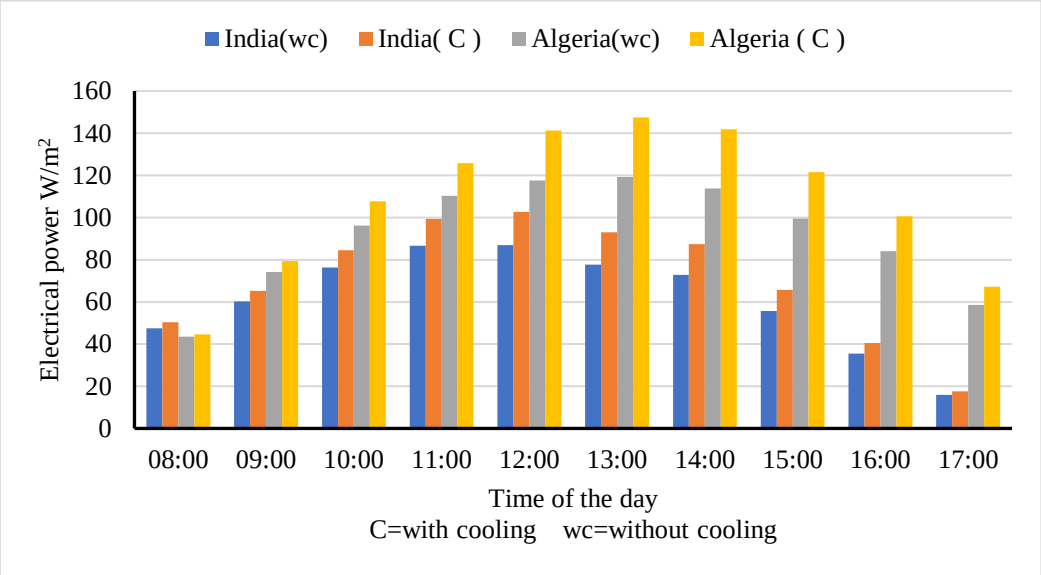

Figure 5.16: Comparison of the hourly specific electric power for the two sites.

For a convention PV module under climatic data of Algeria, the minimum electrical power of 43 W/m^2 was registered at 8:00 Am while the maximum power of 119 W/m^2 was realized at 1:00 Pm. It was observed that the electrical power produced varies nearly linearly with solar irradiation. For the studied geographical locations, the maximum possible electric power generated under the studied climatic conditions when the PVT/PCM-III was employed is 102.7 W/m^2 and 148W/m^2 for India and Algeria, respectively.

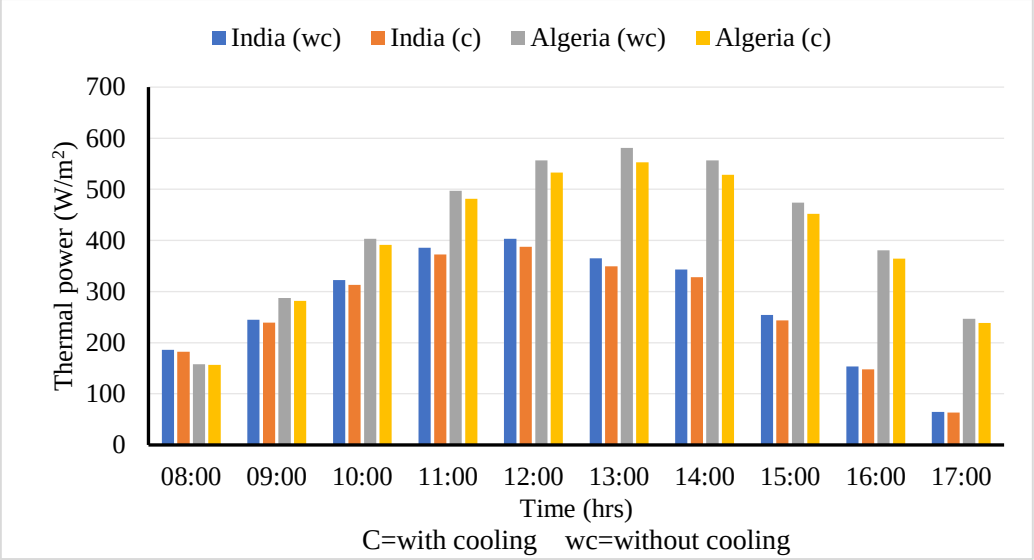

Figure 5.17: Comparison of the hourly specific thermal power for the two sites.

A daily hourly average of 14.9% increase in electrical power is registered in Algeria by use of PVT/PCM-III than conventional PV module while thermal power decreased by 3.9%. For a site in India, minimum electrical power of 17.8W/m^2 was realized at 5:00 Pm while the maximum electrical power of 102.7 W/m^2 was realized at noon with PVT/PCM-III. The module exhibits higher electrical power in Algeria and more energy is lost as heat in India.

CHAPTER 6.

CONCLUSION

In this work, a comparative pilot study of the thermal performance of four solar module configurations was analysed based on the solar irradiation of Uganda. The studied solar module configurations included a conventional PVT module, a coupled PV with PCM material PVT/PCM-I, a PV coupled with internally finned PCM, PVT/PCM-II, and a combined cooling effect of the PCM and a cooling duct coupled onto a PV module, PVT/PCM-III. A detailed thermal analysis was carried out through various thermal parameters and governing equations. To evaluate the thermal performance of the PV systems, a thermal model was developed, numerically solved, and validated through the various published results in the literature. From the pilot study, the following inferences can be drawn:

- When the melting point PCM is close to the Standard test condition's temperature, the system's effectiveness is high. A higher melting point PCM lowers the cooking effect of the PCM.
- The presence of high conductivity copper fins in the PCM domain increases the surface area for heat transfer and acts as pressure relief when the PCM is undergoing a phase transition from liquid to solid.
- Application of a cooling duct as seen in PVT/PCM-III contributes minimal increases in efficiency but allows for a retarded solid-liquid phase transition.

To ascertain the environmental conditions under which the proposed cooling is effective, PVT/PCM-III module configuration which exhibited a high-efficiency value of 18.98%, was selected for evaluation for the two selected sites of Algiers site and Indian Institute of Technology-Delhi. A detailed study using the daily climatic data for the selected places was carried out and the following inferences were drawn.

- When the temperature of the ambient air is lower than the PCM melting temperature, the system's effectiveness is high while in areas where the ambient air temperature is

equal to or slightly higher than the melting temperature of the PCM, systems modifications are required to cool the incoming cooling air.

- The studied PVT/PCM-III is applicable in a coastal Mediterranean climate where the daily hourly ambient air temperature is less than 29°C.

An experimental study based on the numerical findings is proposed for any researcher who would wish to undertake a similar study.

REFERENCES

[1] IRENA, “A Renewable Energy Roadmap Report,” *Irena*, no. June, p. 173, 2014.

[2] O. Aboelwafa, S. E. K. Fateen, A. Soliman, and I. M. Ismail, “A review on solar Rankine cycles: Working fluids, applications, and cycle modifications,” *Renew. Sustain. Energy Rev.*, vol. 82, no. February, pp. 868–885, 2018, doi: 10.1016/j.rser.2017.09.097.

[3] N. Journal, “UNIVERSITÀ DEGLI STUDI DI PADOVA Dipartimento di Scienze Chimiche,” no. Iii, 2014.

[4] Hannah E. Murdock Duncan Gibb Thomas André, *Renewables 2019 Global Status Report*, vol. 8, no. 3. 2019.

[5] T. Saga, “Advances in crystalline silicon solar cell technology for industrial mass production,” *NPG Asia Mater.*, vol. 2, no. 3, pp. 96–102, 2010, doi: 10.1038/asiamat.2010.82.

[6] N. Kannan and D. Vakeesan, “Solar energy for future world: - A review,” *Renew. Sustain. Energy Rev.*, vol. 62, pp. 1092–1105, 2016, doi: 10.1016/j.rser.2016.05.022.

[7] I. M. Bugaje, “Renewable energy for sustainable development in Africa: A review,” *Renew. Sustain. Energy Rev.*, vol. 10, no. 6, pp. 603–612, 2006, doi: 10.1016/j.rser.2004.11.002.

[8] B. Twomey, P. A. Jacobs, and H. Gurgenci, “Dynamic performance estimation of small-scale solar cogeneration with an organic Rankine cycle using a scroll expander,” *Appl. Therm. Eng.*, vol. 51, no. 1–2, pp. 1307–1316, 2013, doi: 10.1016/j.applthermaleng.2012.06.054.

[9] T. Film and S. Cells, “PhD Thesis Modeling of High Power Conversion Efficiency Thin Film Solar Cells.”

[10] J. & Bartlett, “済無No Title No Title,” *J. Chem. Inf. Model.*, vol. 53, no. 9, pp. 1689–1699, 2013.

[11] J. Siecker, K. Kusakana, and B. P. Numbi, “A review of solar photovoltaic systems cooling technologies,” *Renew. Sustain. Energy Rev.*, vol. 79, no. November, pp. 192–203, 2017, doi: 10.1016/j.rser.2017.05.053.

[12] A. R. Jordehi, “Parameter estimation of solar photovoltaic (PV) cells: A review,” *Renew. Sustain. Energy Rev.*, vol. 61, pp. 354–371, 2016, doi: 10.1016/j.rser.2016.03.049.

[13] K. Ranabhat, L. Patrikeev, A. A. evna Revina, K. Andrianov, V. Lapshinsky, and E. Sofronova, “An introduction to solar cell technology,” *J. Appl. Eng. Sci.*, vol. 14, no. 4, pp. 481–491, 2016, doi: 10.5937/jaes14-10879.

[14] M. Tucci and M. Izzi, “High efficiency monocrystalline silicon solar cells: reaching

the theoretical limit," no. August, pp. 745–763, 2013.

[15] J. F. Geisz, D. J. Friedman, J. M. Olson, C. Kramer, A. Kibbler, and S. R. Kurtz, "New materials for future generations of III-V solar cells," vol. 372, no. March 2008, pp. 372–377, 2009, doi: 10.1063/1.57984.

[16] N. Savvakis and T. Tsoutsos, "Theoretical design and experimental evaluation of a PV+PCM system in the mediterranean climate," *Energy*, vol. 220, p. 119690, 2021, doi: 10.1016/j.energy.2020.119690.

[17] A. A and N. John, "Performance Evaluation of On-Grid and Off-Grid Solar Photovoltaic Systems," *Ijireeice*, no. March, pp. 20–23, 2015, doi: 10.17148/ijireeice.2015.3205.

[18] D. A. Quansah, M. S. Adaramola, and L. D. Mensah, "Solar Photovoltaics in Sub-Saharan Africa - Addressing Barriers, Unlocking Potential," *Energy Procedia*, vol. 106, pp. 97–110, 2016, doi: 10.1016/j.egypro.2016.12.108.

[19] G. TK and V. Raj, "Use of phase change material (PCM) for the improvement of thermal performance of cold storage," *MOJ Curr. Res. Rev.*, vol. 1, no. 2, pp. 49–61, 2018, doi: 10.15406/mojcrr.2018.01.00010.

[20] M. Emam, S. Ookawara, and M. Ahmed, "Performance study and analysis of an inclined concentrated photovoltaic-phase change material system," vol. 150, pp. 229–245, 2017.

[21] A. I. A. AL-Musawi, A. Taheri, A. Farzanehnia, M. Sardarabadi, and M. Passandideh-Fard, "Numerical study of the effects of nanofluids and phase-change materials in photovoltaic thermal (PVT) systems," *J. Therm. Anal. Calorim.*, vol. 137, no. 2, pp. 623–636, 2019, doi: 10.1007/s10973-018-7972-6.

[22] S. Meyers, "Energy Demand in the Developing Countries : Towards a Better Understanding Lee Schipper , Jayant Sathaye , Steven Meyers," no. March, 2014.

[23] S. Sorrell, "Reducing energy demand: A review of issues, challenges and approaches," *Renew. Sustain. Energy Rev.*, vol. 47, pp. 74–82, 2015, doi: 10.1016/j.rser.2015.03.002.

[24] F. Fuel, E. Utilization, G. Gas, and B. Zohuri, "Nuclear fuel cycle and decommission- ing Energy-management solutions for mi- crogrids," 2020.

[25] A. J. Jarvis, D. T. Leedal, and C. N. Hewitt, "Climate-society feedbacks and the avoidance of dangerous climate change," *Nat. Clim. Chang.*, vol. 2, no. 9, pp. 668–671, 2012, doi: 10.1038/nclimate1586.

[26] A. McCrone, U. Moslener, F. D'Estais, C. Grüning, and M. Emmerich, "Global Trends In Renewable Energy Investment 2020," p. 80, 2020.

[27] A. Belward *et al.*, *Renewable energies in Africa: Current knowledge*, no. June 2014. 2011.

[28] Y. Wolde-Rufael, "Energy demand and economic growth: The African experience,"

J. Policy Model., vol. 27, no. 8, pp. 891–903, 2005, doi: 10.1016/j.jpolmod.2005.06.003.

[29] M. Mccaskill and S. Angus, “Tyne Polytechnic Phil O ’ Keefe,” pp. 311–312, 1988.

[30] J. Widén and J. Munkhammar, *Solar Radiation Theory*. 2019.

[31] M. Grtzel and J. E. Moser, “Solar Energy Conversion,” *Electron Transf. Chem.*, vol. 5, no. March, pp. 589–644, 2008, doi: 10.1002/9783527618248.ch76.

[32] B. Padmanabhan, “MODELING OF SOLAR CELLS,” 「ジャーナル」, vol. المجلد 49, no. 1, p. 11, 2008.

[33] D. Henner and REN21, *Ren21*. 2017.

[34] X. Zhang, C. Ma, X. Song, Y. Zhou, and W. Chen, “The impacts of wind technology advancement on future global energy,” *Appl. Energy*, vol. 184, pp. 1033–1037, 2016, doi: 10.1016/j.apenergy.2016.04.029.

[35] R. Saidur, M. R. Islam, N. A. Rahim, and K. H. Solangi, “A review on global wind energy policy,” *Renew. Sustain. Energy Rev.*, vol. 14, no. 7, pp. 1744–1762, 2010, doi: 10.1016/j.rser.2010.03.007.

[36] J. I. Lewis and R. H. Wiser, “Fostering a renewable energy technology industry: An international comparison of wind industry policy support mechanisms,” *Energy Policy*, vol. 35, no. 3, pp. 1844–1857, 2007, doi: 10.1016/j.enpol.2006.06.005.

[37] J. Tester, “Congressional Testimony for,” pp. 1–13, 2007.

[38] E. Barbier, “Geothermal energy technology and current status: An overview,” *Renew. Sustain. Energy Rev.*, vol. 6, no. 1–2, pp. 3–65, 2002, doi: 10.1016/S1364-0321(02)00002-3.

[39] I. B. Fridleifsson, “Geothermal energy for the benefit of the people,” *Renew. Sustain. Energy Rev.*, vol. 5, no. 3, pp. 299–312, 2001, doi: 10.1016/S1364-0321(01)00002-8.

[40] J. W. Lund, D. H. Freeston, and T. L. Boyd, “Direct utilization of geothermal energy 2010 worldwide review,” *Geothermics*, vol. 40, no. 3, pp. 159–180, 2011, doi: 10.1016/j.geothermics.2011.07.004.

[41] M. Balat and G. Ayar, “Biomass energy in the world, use of biomass and potential trends,” *Energy Sources*, vol. 27, no. 10, pp. 931–940, 2005, doi: 10.1080/00908310490449045.

[42] C. B. Field, J. E. Campbell, and D. B. Lobell, “Biomass energy: the scale of the potential resource,” *Trends Ecol. Evol.*, vol. 23, no. 2, pp. 65–72, 2008, doi: 10.1016/j.tree.2007.12.001.

[43] T. Karlsson, “Cooling integrated solar panels using Phase Changing Materials,” no. June, 2018.

[44] M. GREEN *et al.*, “Solar cell efficiency tables (version 40),” *Ieee Trans Fuzzy Syst*,

vol. 20, no. 6, pp. 1114–1129, 2012, doi: 10.1002/pip.

[45] B. L. Sater, “Solar cell,” *Phys. Today*, vol. 33, no. 3, pp. 116–117, 1980, doi: 10.1063/1.2913977.

[46] D. E. Carlson and C. R. Wronski, “Amorphous silicon solar cell,” *Appl. Phys. Lett.*, vol. 28, no. 11, pp. 671–673, 1976, doi: 10.1063/1.88617.

[47] S. C. Chien and F. C. Chenb, “Polymer solar cells,” *Polym. Electron.*, no. October 2007, pp. 179–222, 2013, doi: 10.4032/9789814364041.

[48] G. Li, R. Zhu, and Y. Yang, “Polymer solar cells,” *Nat. Photonics*, vol. 6, no. 3, pp. 153–161, 2012, doi: 10.1038/nphoton.2012.11.

[49] T. Sogabe, Q. Shen, and K. Yamaguchi, “Recent progress on quantum dot solar cells: a review,” *J. Photonics Energy*, vol. 6, no. 4, p. 040901, 2016, doi: 10.1117/1.jpe.6.040901.

[50] M. Grätzel, “Dye-sensitized solar cells,” *J. Photochem. Photobiol. C Photochem. Rev.*, vol. 4, no. 2, pp. 145–153, 2003, doi: 10.1016/S1389-5567(03)00026-1.

[51] E. Skoplaki and J. A. Palyvos, “On the temperature dependence of photovoltaic module electrical performance: A review of efficiency/power correlations,” *Sol. Energy*, vol. 83, no. 5, pp. 614–624, 2009, doi: 10.1016/j.solener.2008.10.008.

[52] T. A. Salaoru *et al.*, “treatment Modelling of systems with multiple energy carriers in buildings Numerical study of air cooling photovoltaic panels using heat sinks,” 2016.

[53] H. A. Nasef, S. A. Nada, and H. Hassan, “Integrative passive and active cooling system using PCM and nanofluid for thermal regulation of concentrated photovoltaic solar cells,” *Energy Convers. Manag.*, vol. 199, no. September, p. 112065, 2019, doi: 10.1016/j.enconman.2019.112065.

[54] A. Royne, C. J. Dey, and D. R. Mills, “Cooling of photovoltaic cells under concentrated illumination: A critical review,” *Sol. Energy Mater. Sol. Cells*, vol. 86, no. 4, pp. 451–483, 2005, doi: 10.1016/j.solmat.2004.09.003.

[55] K. Araki, H. Uozumi, and M. Yamaguchi, “A simple passive cooling structure and its heat analysis for 500 X concentrator PV module,” *Conf. Rec. IEEE Photovolt. Spec. Conf.*, pp. 1568–1571, 2002, doi: 10.1109/pvsc.2002.1190913.

[56] M. Jaworski, “Thermal performance of heat spreader for electronics cooling with incorporated phase change material,” *Appl. Therm. Eng.*, vol. 35, no. 1, pp. 212–219, 2012, doi: 10.1016/j.applthermaleng.2011.10.036.

[57] M. R. Shaeri and R. W. Bonner, “Analytical heat transfer model for laterally perforated-finned heat sinks,” *Int. J. Heat Mass Transf.*, vol. 131, pp. 1164–1173, 2019, doi: 10.1016/j.ijheatmasstransfer.2018.11.138.

[58] “Introduction to Engineering Heat Transfer.”

[59] Hari Raghavan J and Rangu P, “A Study and Analysis on the Thermal Performance

of a Pin Fin Heatsink for Natural Convection using CFD," *Int. J. Eng. Res.*, vol. V6, no. 05, 2017, doi: 10.17577/ijertv6is050563.

[60] A. Uday Kumar, A. Javed, and S. K. Dubey, "Material Selection for Microchannel Heatsink: Conjugate Heat Transfer Simulation," *IOP Conf. Ser. Mater. Sci. Eng.*, vol. 346, no. 1, 2018, doi: 10.1088/1757-899X/346/1/012024.

[61] A. Soni, "Study of Thermal Performance between Plate-fin, Pin-fin and Elliptical Fin Heat Sinks in Closed Enclosure under Natural Convection," *Int. Adv. Res. J. Sci. Eng. Technol. ISO*, vol. 3297, no. 11, pp. 133–139, 2007, doi: 10.17148/IARJSET.2016.31126.

[62] A. Hasan, S. J. McCormack, M. J. Huang, and B. Norton, "Evaluation of phase change materials for thermal regulation enhancement of building integrated photovoltaics," *Sol. Energy*, vol. 84, no. 9, pp. 1601–1612, 2010, doi: 10.1016/j.solener.2010.06.010.

[63] P. Ruano *et al.*, "We are IntechOpen , the world ' s leading publisher of Open Access books Built by scientists , for scientists TOP 1 %," *Intech*, no. tourism, p. 13, 2016.

[64] . K. A. T., "Review on Latent Heat Storage and Problems Associated With Phase Change Materials," *Int. J. Res. Eng. Technol.*, vol. 04, no. 10, pp. 176–182, 2015, doi: 10.15623/ijret.2015.0410030.

[65] K. S. Pascha, "The use of phase-change-material as cooling-strategy for buildings in the Chilean climate," *Int. J. Low Carbon Technol.*, vol. 3, no. 2, pp. 101–109, 2008, doi: 10.1093/ijlct/3.2.101.

[66] S. Khare, M. Dell'Amico, C. Knight, and S. McGarry, "Selection of materials for high temperature latent heat energy storage," *Sol. Energy Mater. Sol. Cells*, vol. 107, pp. 20–27, 2012, doi: 10.1016/j.solmat.2012.07.020.

[67] A. Hoshi, D. R. Mills, A. Bittar, and T. S. Saitoh, "Screening of high melting point phase change materials (PCM) in solar thermal concentrating technology based on CLFR," *Sol. Energy*, vol. 79, no. 3, pp. 332–339, 2005, doi: 10.1016/j.solener.2004.04.023.

[68] J. Q. Zhong, A. T. Fragoso, A. J. Wells, and J. S. Wettlaufer, *Finite-sample-size effects on convection in mushy layers*, vol. 704. 2012.

[69] R. Adinberg, D. Zvegilsky, and M. Epstein, "Heat transfer efficient thermal energy storage for steam generation," *Energy Convers. Manag.*, vol. 51, no. 1, pp. 9–15, 2010, doi: 10.1016/j.enconman.2009.08.006.

[70] M. Sardarabadi, M. Passandideh-Fard, M. J. Maghrebi, and M. Ghazikhani, "Experimental study of using both ZnO/ water nanofluid and phase change material (PCM) in photovoltaic thermal systems," *Sol. Energy Mater. Sol. Cells*, vol. 161, no. November 2016, pp. 62–69, 2017, doi: 10.1016/j.solmat.2016.11.032.

[71] M. J. Huang, P. C. Eames, B. Norton, and N. J. Hewitt, "Natural convection in an

internally finned phase change material heat sink for the thermal management of photovoltaics," *Sol. Energy Mater. Sol. Cells*, vol. 95, no. 7, pp. 1598–1603, 2011, doi: 10.1016/j.solmat.2011.01.008.

[72] S. Manikandan, C. Selvam, N. Poddar, K. Pranjyal, R. Lamba, and S. C. Kaushik, "Thermal management of low concentrated photovoltaic module with phase change material," *J. Clean. Prod.*, vol. 219, pp. 359–367, 2019, doi: 10.1016/j.jclepro.2019.02.086.

[73] Z. Arifin, D. D. D. P. Tjahjana, S. Hadi, R. A. Rachmanto, G. Setyohandoko, and B. Sutanto, "Numerical and experimental investigation of air cooling for photovoltaic panels using aluminum heat sinks," *Int. J. Photoenergy*, vol. 2020, 2020, doi: 10.1155/2020/1574274.

[74] F. Al-Ajmi, D. L. Loveday, and V. I. Hanby, "The cooling potential of earth-air heat exchangers for domestic buildings in a desert climate," *Build. Environ.*, vol. 41, no. 3, pp. 235–244, 2006, doi: 10.1016/j.buildenv.2005.01.027.

[75] M. I. Hasan, S. W. Noori, and A. J. Shkarah, "Parametric study on the performance of the earth-to-air heat exchanger for cooling and heating applications," *Heat Transf. - Asian Res.*, vol. 48, no. 5, pp. 1805–1829, 2019, doi: 10.1002/htj.21458.

[76] M. K. Ghosal, G. N. Tiwari, and N. S. L. Srivastava, "Thermal modeling of a greenhouse with an integrated earth to air heat exchanger: An experimental validation," *Energy Build.*, vol. 36, no. 3, pp. 219–227, 2004, doi: 10.1016/j.enbuild.2003.10.006.

[77] S. A. Nada, D. H. El-Nagar, and H. M. S. Hussein, "Improving the thermal regulation and efficiency enhancement of PCM-Integrated PV modules using nano particles," *Energy Convers. Manag.*, vol. 166, no. January, pp. 735–743, 2018, doi: 10.1016/j.enconman.2018.04.035.

[78] "RT25HC," p. 2020, 2020.

[79] D. Okello, J. Mubiru, and E. J. K. Banda, "Availability of direct solar radiation in Uganda," *30th ISES Bienn. Sol. World Congr. 2011, SWC 2011*, vol. 5, pp. 3554–3563, 2011, doi: 10.18086/swc.2011.24.22.

[80] Q. Kang *et al.*, "Materials Characterization Microstructure and thermal properties of copper – diamond composites with tungsten carbide coating on diamond particles," *Mater. Charact.*, vol. 105, pp. 18–23, 2015, doi: 10.1016/j.matchar.2014.07.025.

[81] B. Niezgoda-Zelasko, "The Enthalpy-porosity Method Applied to the Modelling of the Ice Slurry Melting Process during Tube Flow," *Procedia Eng.*, vol. 157, pp. 114–121, 2016, doi: 10.1016/j.proeng.2016.08.346.

[82] H. A. Nasef, S. A. Nada, and H. Hassan, "Integrative passive and active cooling system using PCM and nano fl uid for thermal regulation of concentrated photovoltaic solar cells," vol. 199, no. June, 2019.

[83] H. Shmueli, G. Ziskind, and R. Letan, "Melting in a vertical cylindrical tube:

Numerical investigation and comparison with experiments," *Int. J. Heat Mass Transf.*, vol. 53, no. 19–20, pp. 4082–4091, 2010, doi: 10.1016/j.ijheatmasstransfer.2010.05.028.

[84] V. Voloshin, Y. K. Chen, and R. K. Calay, "A comparison of turbulence models in airship steady-state CFD simulations," no. October, 2012.

[85] T. R. Taha, *An Introduction to Parallel Computational Fluid Dynamics*, vol. 6, no. 4. 2005.

[86] M. E. A. Slimani, M. Amirat, I. Kurucz, S. Bahria, A. Hamidat, and W. B. Chaouch, "A detailed thermal-electrical model of three photovoltaic/thermal (PV/T) hybrid air collectors and photovoltaic (PV) module: Comparative study under Algiers climatic conditions," *Energy Convers. Manag.*, vol. 133, pp. 458–476, 2017, doi: 10.1016/j.enconman.2016.10.066.

[87] J. Zhou, Q. Yi, Y. Wang, and Z. Ye, "Temperature distribution of photovoltaic module based on finite element simulation," *Sol. Energy*, vol. 111, pp. 97–103, 2015, doi: 10.1016/j.solener.2014.10.040.

[88] S. Dubey, J. N. Sarvaiya, and B. Seshadri, "Temperature dependent photovoltaic (PV) efficiency and its effect on PV production in the world - A review," *Energy Procedia*, vol. 33, pp. 311–321, 2013, doi: 10.1016/j.egypro.2013.05.072.

[89] İ. Ceylan *et al.*, "Determination of the heat transfer coefficient of PV panels," *Energy*, vol. 175, pp. 978–985, 2019, doi: 10.1016/j.energy.2019.03.152.

[90] C. G. Popovici, S. V. Hudişteanu, T. D. Mateescu, and N. C. Cherecheş, "Efficiency Improvement of Photovoltaic Panels by Using Air Cooled Heat Sinks," *Energy Procedia*, vol. 85, no. November 2015, pp. 425–432, 2016, doi: 10.1016/j.egypro.2015.12.223.

[91] P. Raghuraman, "Design considerations for flat-plate- photovoltaic/thermal collectors," vol. 35, no. 3, pp. 227–241, 1985.

[92] H. G. Teo, P. S. Lee, and M. N. A. Hawlader, "An active cooling system for photovoltaic modules," *Appl. Energy*, vol. 90, no. 1, pp. 309–315, 2012, doi: 10.1016/j.apenergy.2011.01.017.

[93] A. Radwan, S. Ookawara, and M. Ahmed, "Analysis and simulation of concentrating photovoltaic systems with a microchannel heat sink," *Sol. Energy*, vol. 136, pp. 35–48, 2016, doi: 10.1016/j.solener.2016.06.070.

[94] H. Bencheikh and Y. Daoudji, "Numerical Investigation of a Coupled Passive Cooling System Earth to Air Heat Exchange and Solar Chimney in Hot Arid Zone," *Innov. Energy Res.*, vol. 07, no. 01, pp. 1–7, 2018, doi: 10.4172/2576-1463.1000188.

[95] T. S. Bisoniya, "Design of earth–air heat exchanger system," *Geotherm. Energy*, vol. 3, no. 1, 2015, doi: 10.1186/s40517-015-0036-2.

[96] M. Sardarabadi, M. Passandideh-fard, M. Maghrebi, and M. Ghazikhani,

"crossmark," vol. 161, no. November 2016, pp. 62–69, 2017.

[97] B. Kamkari, H. Shokouhmand, and F. Bruno, "Experimental investigation of the effect of inclination angle on convection-driven melting of phase change material in a rectangular enclosure," *Int. J. Heat Mass Transf.*, vol. 72, pp. 186–200, 2014, doi: 10.1016/j.ijheatmasstransfer.2014.01.014.

[98] S. Cho *et al.*, "Effects of infrared radiation and heat on human skin aging in vivo," *J. Investig. Dermatology Symp. Proc.*, vol. 14, no. 1, pp. 15–19, 2009, doi: 10.1038/jidsymp.2009.7.

[99] R. Velraj, R. V. Seeniraj, B. Hafner, C. Faber, and K. Schwarzer, "Heat transfer enhancement in a latent heat storage system," *Sol. Energy*, vol. 65, no. 3, pp. 171–180, 1999, doi: 10.1016/S0038-092X(98)00128-5.

[100] A. S. Joshi, A. Tiwari, G. N. Tiwari, I. Dincer, and B. V. Reddy, "Performance evaluation of a hybrid photovoltaic thermal (PV/T) (glass-to-glass) system," *Int. J. Therm. Sci.*, vol. 48, no. 1, pp. 154–164, 2009, doi: 10.1016/j.ijthermalsci.2008.05.001.

[101] M. E. A. Slimani, M. Amirat, I. Kurucz, S. Bahria, A. Hamidat, and W. B. Chaouch, "A detailed thermal-electrical model of three photovoltaic/thermal (PV/T) hybrid air collectors and photovoltaic (PV) module: Comparative study under Algiers climatic conditions," *Energy Convers. Manag.*, vol. 133, pp. 458–476, 2017, doi: 10.1016/j.enconman.2016.10.066.